Near-term acceleration of hydroclimatic change in the western U.S.

Moetasim Ashfaq,[1,2,3] Subimal Ghosh,[4] Shih-Chieh Kao,[1] Laura C. Bowling,[5] Philip Mote,[6] Danielle Touma,[1] Sara A. Rauscher,[7] and Noah S. Diffenbaugh[2,3]

Received 30 January 2013; revised 3 September 2013; accepted 5 September 2013; published 1 October 2013.

[1] Given its large population, vigorous and water-intensive agricultural industry, and important ecological resources, the western United States presents a valuable case study for examining potential near-term changes in regional hydroclimate. Using a high-resolution, hierarchical, five-member ensemble modeling experiment that includes a global climate model (Community Climate System Model), a regional climate model (RegCM), and a hydrological model (Variable Infiltration Capacity model), we find that increases in greenhouse forcing over the next three decades result in an acceleration of decreases in spring snowpack and a transition to a substantially more liquid-dominated water resources regime. These hydroclimatic changes are associated with increases in cold-season days above freezing and decreases in the cold-season snow-to-precipitation ratio. The changes in the temperature and precipitation regime in turn result in shifts toward earlier snowmelt, base flow, and runoff dates throughout the region, as well as reduced annual and warm-season snowmelt and runoff. The simulated hydrologic response is dominated by changes in temperature, with the ensemble members exhibiting varying trends in cold-season precipitation over the next three decades but consistent negative trends in cold-season freeze days, cold-season snow-to-precipitation ratio, and 1 April snow water equivalent. Given the observed impacts of recent trends in snowpack and snowmelt runoff, the projected acceleration of hydroclimatic change in the western U.S. has important implications for the availability of water for agriculture, hydropower, and human consumption, as well as for the risk of wildfire, forest die-off, and loss of riparian habitat.

Citation: Ashfaq, M., S. Ghosh, S.-C. Kao, L. C. Bowling, P. Mote, D. Touma, S. A. Rauscher, and N. S. Diffenbaugh (2013), Near-term acceleration of hydroclimatic change in the western U.S., *J. Geophys. Res. Atmos.*, *118*, 10,676–10,693, doi:10.1002/jgrd.50816.

1. Introduction

[2] The 11 U.S. States that fall entirely west of 100°W are home to 23% of the U.S. population [*USCB*, 2011], 21% of the U.S. agricultural value [*USDA, E. R. S.*, 2011], and a diverse array of ecosystems [*Myers et al.*, 2000]. The availability of water in much of the western U.S. is highly dependent on snowmelt, in part because much of the western U.S. receives the majority of precipitation during the cold season [*Mock*, 1996] and in part because runoff from snowmelt is far more gradual than from rainfall. As a result, many of the management systems that provide water for agriculture, hydropower, and human consumption have been built around the "natural reservoir" provided by the snowpack [*Hamlet and Lettenmaier*, 1999]. Ecosystems are likewise reliant on this natural reservoir, including the critical moisture that it provides during the dry warm-season months [e.g., *Hayhoe et al.*, 2004; *Rood et al.*, 2008].

[3] While there is heterogeneity within the western U.S., hydroclimatic observations show trends toward decreasing spring snowpack at 75% of sites in mountainous areas [*Mote et al.*, 2005] and earlier dates of snowmelt runoff [*Aguado et al.*, 1992; *Cayan et al.*, 2001; *Dettinger and Cayan*, 1995; *McCabe and Clark*, 2005; *Rauscher et al.*, 2008; *Stewart et al.*, 2004]. These changes have had important impacts on the western U.S., including increasing risk of pest infestation [*Kurz et al.*, 2008], forest die-off [*Kelly and Goulden*, 2008] and wildfires [*Westerling et al.*, 2006], and increasing stress on riparian ecosystems [*Rood et al.*, 2005]. Previous work has quantitatively attributed observed trends in snowpack and river flow to anthropogenic global warming [*Barnett et al.*, 2008; *Pierce et al.*, 2008]. In addition, global warming that is projected for the middle to late 21st century is expected to cause decreases in snow

[1]Oak Ridge National Laboratory, Oak Ridge, Tennessee, USA.
[2]Woods Institute for the Environment and Department of Environmental Earth System Science, Stanford University, Stanford, California, USA.
[3]Purdue Climate Change Research Center and Department of Earth, Atmospheric and Planetary Sciences, Purdue University, West Lafayette, Indiana, USA.
[4]Department of Civil Engineering, Indian Institute of Technology, Bombay, India.
[5]Purdue Climate Change Research Center and Department of Agronomy, Purdue University, West Lafayette, Indiana, USA.
[6]Oregon Climate Change Research Institute and Oregon Climate Services, Oregon State University, Corvallis, Oregon, USA.
[7]Department of Geography, University of Delaware, Newark, Delaware, USA.

Corresponding author: M. Ashfaq, Oak Ridge National Laboratory, PO Box MS6301, Oak Ridge, TN 37831-6301, USA. (mashfaq@ornl.gov)

2169-897X/13/10.1002/jgrd.50816

accumulation and shifts toward earlier snowmelt runoff [*Adam et al*., 2009; *Casola et al*., 2009; *Gao et al*., 2011; *Hamlet et al*., 2005; *Leung and Ghan*, 1999; *Leung et al*., 2004; *Maurer*, 2007; *Mote et al*., 2005; *Rasmussen et al*., 2011; *Rauscher et al*., 2008; *Stewart et al*., 2004; *Wi et al*., 2012].

[4] Despite this large body of work, the pace and magnitude of hydroclimatic change over the near-term decades remains a key question for much of the western U.S. The fact that global warming is likely to continue even after stabilization of greenhouse gas concentrations [e.g., *Matthews and Caldeira*, 2008; *Matthews and Weaver*, 2010; *Solomon et al*., 2009; *Wigley*, 2005] and that substantial regional climate change is likely to occur in response to as little as 1°C of additional global warming [e.g., *Clark et al*., 2010; *Diffenbaugh and Ashfaq*, 2010; *Diffenbaugh and Scherer*, 2011] increases the likelihood that some climate change adaptation will be required over the near-term decades [*Carter et al*., 2007]. In addition, the near-term decades encompass the planning horizon for many water-resource-infrastructure design decisions [e.g., *WAC*, 2010]. However, the interacting effects of temperature and precipitation complicate near-term projections of hydroclimatic change in regions where water resources are strongly dependent on snowpack [*Stewart*, 2009], particularly given the substantial uncertainty in near-term changes in regional precipitation [*Hawkins and Sutton*, 2010].

[5] In the present study, we employ a high-resolution ensemble experiment to quantify possible changes in snow-dominated water resources in the western U.S. over the 2000–2039 period. While there have been some studies over the western U.S. that provide a future snow outlook under increasing greenhouse forcing using statistical downscaling of general circulation models (GCMs) [e.g., *Payne et al*., 2004; *Stewart et al*., 2004], this is—to the best of our knowledge—the first time that a multimember process-based high-resolution climate modeling system has been used to provide future snow projections. Projections using statistical downscaling are limited in many respects. First, the relationships between the large-scale atmospheric variables (predictors) and the local climate characteristics (predictands) is assumed to be stationary under future climate change, meaning that future projections based on the statistical downscaling of the GCMs will fail to account for the changes in snow hydrology that are driven by the variations in the relationships between the large-scale predictors and local-scale predictands. Second, future projections are often sensitive to the choice of the predictors in the statistical model as well as to the ability of the GCMs to simulate those predictors. Third, statistical downscaling cannot accommodate many regional factors that may influence the fine-scale hydrological responses, particularly in the areas of complex terrain. These fine-scale processes—such as topographically controlled snow-albedo feedbacks—have been identified as a key regulator of the regional cold-season temperature response [e.g., *Rauscher et al*., 2008], and the effects of such sub-GCM-scale processes on the local temperature response to global warming will not be reflected in statistical downscaling approaches. However, we do note that our modeling strategy is a combination of process-based hydroclimate modeling and statistics-based bias correction and spatial disaggregation and is therefore not fully immune to the errors originating from the lack of the physical representation of fine-scale processes.

[6] Our motivation for this near-term high-resolution ensemble experiment is threefold. First, the expected global warming over the next three decades falls within 2°C above the preindustrial baseline [*Meehl et al*., 2007b], motivating examination of potential climatic changes that require adaptation action on this near-term timescale [e.g., *Carter et al*., 2007]. Second, the topographic complexity of the western U.S. can influence the magnitude of warming-induced changes in winter temperature and timing of snowmelt-dominated runoff [*Leung and Ghan*, 1999; *Rauscher et al*., 2008], motivating application of a high-resolution climate modeling system to represent more accurately those fine-scale climate processes. Third, climate system variability can exert a strong influence on the temporal evolution of regional temperature and precipitation over the near-term decades [e.g., *Hawkins and Sutton*, 2010]. Because snow is sensitive to both temperature and precipitation, this variability can have a particularly strong imprint on decadal trends in snow accumulation and melt [e.g., *Scherrer et al*., 2004]. However, although multimember, single-model ensemble experiments are common in the GCM literature [e.g., *Murphy et al*., 2004], very few multimember, single-model, high-resolution ensemble experiments exist (e.g., the North American Regional Climate Change Assessment Program experiment is focused on multimodel, single-realization experiments; [*Mearns et al*., 2009]), motivating the application of our high-resolution ensemble to test the influence of internal climate system variability on the near-term evolution of hydroclimatic change in the western U.S.

2. Models and Methods

2.1. Climate Model Experiments

[7] We generate a five-member, high-resolution, climate model ensemble by nesting one high-resolution realization of the International Centre for Theoretical Physics Regional Climate Model Version 3 (RegCM3) within each of five realizations of the Community Climate System Model Version 3 (CCSM3) [*Diffenbaugh and Ashfaq*, 2010; *Diffenbaugh et al*., 2011]. As described below, our nesting covers the period from 1950 to 2039 in the Intergovernmental Panel on Climate Change Special Report on Emission Scenarios (SRES) A1B scenario, with RegCM3 run at 25 km horizontal resolution and 18 levels in the vertical, and CCSM3 run at T85 (1.4°) horizontal resolution and 26 levels in the vertical.

[8] Details of the RegCM3 nested climate model are described in *Pal et al*. [2007]. RegCM3 is a hydrostatic, sigma coordinate, primitive equation, limited-area model. In our configuration, RegCM3 uses the hydrostatic dynamical core from Fifth-Generation Mesoscale Model (MM5) [*Grell et al*., 1994], the radiation package from Community Climate Model Version-3 (CCM3) [*Kiehl et al*., 1996], the Biosphere Atmosphere Transfer Scheme (BATS) 1e land model [*Dickinson et al*., 1993], and the Holtslag boundary layer package [*Holtslag et al*., 1990]. Precipitation processes are parameterized using the Subgrid Explicit Moisture Scheme (SUBEX) scheme of *Pal et al*. [2000] and the cumulus convection parameterization of *Grell* [1993] with the closure assumption of *Fritsch and Chappell* [1980]. RegCM3 has been evaluated over many areas of the globe, including extensive evaluation of the temperature, precipitation,

moisture, runoff, Convective Available Potential Energy (CAPE), and wind fields over the continental U.S. [*Ashfaq et al*., 2010b; *Diffenbaugh and Ashfaq*, 2007; *Diffenbaugh and Ashfaq*, 2010; *Diffenbaugh et al*., 2011; *Diffenbaugh et al*., 2006; *Rauscher et al*., 2008; *Trapp et al*., 2007; *Walker and Diffenbaugh*, 2009].

[9] The CCSM3 realizations are described in *Meehl et al*. [2006]. The five realizations were generated using a standard atmosphere-ocean general circulation model ensemble method, with each realization initialized from a different point in the preindustrial control simulation, and all ensemble realizations prescribed identical atmospheric constituent concentrations over the historical and scenario periods. The five CCSM3 realizations therefore differ only in the atmosphere, land, and ocean conditions at the time of initial industrial-age forcing. The global warming in the CCSM3 A1B ensemble falls near the middle of the Coupled Model Intercomparison Project phase 3 (CMIP3) ensemble, with the CMIP3 ensemble showing warming of 1.0 to 1.7°C above the late 20th century baseline at the end of the 2030s [*Meehl et al*., 2007b] and the CCSM3 ensemble showing warming of 1.1 to 1.3°C [*Meehl et al*., 2006].

[10] We generate the five-member high-resolution ensemble by nesting the RegCM3 grid in each of the five CCSM3 simulations identified by National Center for Atmospheric Research (NCAR) as c, e, bES.01, fES.01, and gES.01. Because the subdaily, three-dimensional atmospheric fields that are necessary for the high-resolution nesting were not saved by NCAR for the CCSM3 ensemble realizations, we rerun the atmospheric component of CCSM3 (CAM3) at the original resolution (T85 with 26 levels in the vertical), prescribing the original monthly CCSM3 sea surface temperatures (SSTs) and sea ice as a bottom boundary condition, as described in *Trapp et al*. [2009] and *Diffenbaugh et al*. [2006]. This "time-slice" approach, which is necessary for generating the high-resolution ensemble simulation, reproduces the original CCSM3 temperature and precipitation fields, with statistically significant seasonal errors primarily confined to the tropics [*Ashfaq et al*., 2010a].

[11] The RegCM3 equal-area grid follows that of *Diffenbaugh et al*. [2005] and covers the full continental U.S. at 25 km horizontal resolution, with 18 levels in the vertical. All of the five RegCM3 realizations use identical model configurations and simulation time steps (75 s), meaning that only the large-scale CCSM3 boundary conditions vary between the RegCM3 members. In each RegCM3 realization, the large-scale atmospheric boundary conditions are updated from the respective CAM3 global atmosphere realization at the RegCM3 lateral boundaries every six simulated hours, and the SST and sea ice boundary conditions are updated from the respective CCSM3 global ocean realization at the RegCM3 lower boundary every simulated month.

[12] The CAM3 integrations are initialized on 1 January 1948, using the respective instantaneous CCSM3 fields as initial conditions, and run continuously through 2039 in the SRES A1B scenario. The RegCM3 integrations are initialized on 1 January 1950, using the respective instantaneous CAM3 atmospheric fields and monthly CCSM3 SSTs as initial conditions, and run continuously through 2039 in the SRES A1B scenario. Both CAM3 and RegCM3 use the same annually varying greenhouse gas concentrations as were applied in the original CCSM3 realizations, with observational values applied over the 20th century period and scenario values applied over the 21st century period. Our analysis begins in 1960, allowing 10 years for RegCM3 equilibration and 12 years for CAM3 equilibration.

2.2. Hydrologic Model Experiments

[13] We employ the Variable Infiltration Capacity (VIC) model [*Cherkauer et al*., 2003] to simulate the hydrologic response to near-term changes in global radiative forcing. We use VIC as opposed to the outputs from the RegCM3 land component (BATS) because VIC is much more sophisticated in its representation of processes that govern fine-scale snow hydrology. Similarly, most of the current generation of GCMs exhibit large discrepancies in the simulation of snow hydrology in regions of complex topography [*Diffenbaugh et al*., 2013]. The VIC model is a distributed macroscale surface water and energy balance model that has been applied over a range of scales, including for the continental U.S. [e.g., *Christensen et al*., 2004; *Vicuna et al*., 2007], and has been previously used to study both past and future hydroclimate change [e.g., *Beyene et al*., 2010; *Christensen et al*., 2004; *Costa-Cabral et al*., 2013; *Hamlet and Lettenmaier*, 1999]. In this study, we employ VIC model version 4.1.1 at one-eighth degree horizontal resolution and 3-hourly simulation time step in energy balance mode (land surface temperature solved by iteration), using daily minimum and maximum temperatures, precipitation, and wind fields. The one-eighth degree configuration is the standard Land Data Assimilation System (LDAS) version used for simulating large domains that allows us to use the input data sets that have been rigorously adjusted to calibrate VIC for larger domains such as the western U.S. [e.g., *Fan et al*., 2011]. We use the *Liang et al*. [1994] scheme for ground heat flux, the *Sun et al*. [1999] algorithm for snow albedo, and a one-dimensional temperature-dependent snow cover model (SNTHRM) algorithm for snow density [*Jordan*, 1991]. Ten snow elevation bands represent subgrid variations in elevation. The elevation of each band is used to lapse the grid cell average temperature, pressure, and precipitation to a more accurate local estimate. The soil hydraulic and thermal parameters, and the depth of soil layers, are identical to those described in *Ashfaq et al*. [2010b].

[14] We generate one VIC model simulation for each of the five RegCM3 simulations. We bias-correct the RegCM3 daily temperature and precipitation fields on the one-eighth degree VIC grid prior to using them as input for the VIC model, as described by *Ashfaq et al*. [2010b]. Using the simple inverse distance weighting technique, we first interpolate both the RegCM3 and observational fields to the VIC one-eighth degree geographical grid. Further, the bias correction is applied to each monthly quantile of precipitation and temperature in each calendar month of the baseline and future periods. In the baseline period, for a given ensemble member, the bias correction corrects each quantile of each calendar month in the simulated time series by mapping it to the corresponding observed quantile. For instance, the warmest January in the simulated data is corrected by the warmest January in the observed data, the warmest February in the simulated data is corrected by the warmest February in the observed data, and so on for all minimum and maximum temperature quantiles of all 12 calendar months. Similarly, the wettest January in the simulated data is corrected by the

wettest January in the observed data, the wettest February in the simulated data is corrected by the wettest February in the observed data, and so on for all precipitation quantiles of all 12 calendar months. In the future period, the change in the magnitude of each quantile (quantile shift) is first calculated in each calendar month as a difference (future minus baseline) for minimum and maximum temperature and as a ratio (future divided by baseline) for precipitation. The bias-corrected future period quantiles are then generated by adding the quantile shifts to the bias-corrected baseline quantiles in the case of minimum temperature and maximum temperature and by multiplying the quantile shift by the bias-corrected baseline quantiles in the case of precipitation. For instance, we add the temperature differences between the maximum January value in the future period and the maximum January value in the baseline period to the maximum January value in the bias-corrected baseline period. Similarly, we multiply the ratio between the wettest January in the future period and the wettest January in the baseline period by the wettest January value in the bias-corrected baseline period. We distribute the monthly correction from each bias-corrected month to the model-simulated daily time series so that the daily distribution is maintained but the aggregate is equal to the bias-corrected monthly mean. This bias correction methodology maintains the changes in temperature and precipitation simulated by the climate model but greatly improves the hydrologic simulation of the historical period relative to that derived using observational daily-scale climate inputs, both by correcting systematic errors in the absolute magnitude of the simulated temperature and precipitation inputs and by improving the spatial detail of the simulated inputs [*Ashfaq et al*., 2010b]. Because we simulate the 40 year period from 2000 to 2039 in the A1B scenario, we use the 40 year period from 1960 to 1999 as our baseline period for bias correction.

[15] For comparison, we also generate one VIC model simulation for each of the five CCSM3 simulations, using the bias-corrected CCSM3 daily temperature and precipitation and original wind fields. Bias correction and spatial disaggregation of the CCSM3 fields in the baseline and future periods is carried out in an identical way to that described above for the RegCM3 fields. We use these CCSM3-driven VIC simulations to understand the sources of errors in the RegCM3-driven VIC simulations in the baseline period and to test the robustness of the simulated hydrological response to increasing greenhouse forcing in the future period. Hereafter, we refer to the RegCM3-driven VIC simulations as the VIC ensemble and the CCSM3-driven VIC simulations as the GCM-VIC ensemble. Additionally, in order to probe the uncertainty in the temperature and precipitation projections of our high-resolution RegCM3 ensemble, we compare the RegCM3 monthly precipitation and temperature fields with those from the Coupled Model Intercomparison Project phase 3 (CMIP3) and phase 5 (CMIP5) multimodel GCM ensembles. We construct a CMIP3 ensemble by selecting "run1" from each of the GCMs archiving both temperature and precipitation data for the baseline and future periods in the A1B experiment (22 in total). Similarly, we construct a CMIP5 ensemble by selecting one run from each of the GCMs archiving temperature and precipitation data for the baseline and future periods in the Representative Concentration Pathway 8.5 (RCP8.5) experiment (33 in total for precipitation and 31 in total for temperature). Because the CMIP5 future period starts from 2006, we use 1960–1999 as the baseline period and 2006–2039 as the future period for these comparisons.

2.3. Observational Data

[16] We employ three observational data sets:

[17] 1. As described in *Mote et al*. [2005] and *Mote* [2006], snow course data corresponding to the period of the baseline simulation are obtained from the California Department of Water Resources (for California) and the Water and Climate Center of the U.S. Department of Agriculture's Natural Resource Conservation Service (for the remaining states).

[18] 2. Monthly runoff observations are obtained from the United States Geological Survey WaterWatch program [*Brakebill et al*., 2011]. WaterWatch runoff is estimated by combining historical flow data collected at U.S. Geological Survey (USGS) streamflow gauges, the respective drainage basin boundaries of the streamflow gauges, and the boundaries of each six-digit hydrologic unit of *Seaber et al*. [1987] (referred to as "HUC06 accounting units"). WaterWatch runoff can therefore be considered a close surrogate to the natural runoff.

[19] 3. Observational monthly temperature and precipitation data are taken from the Parameter-Elevation Regressions on Independent Slopes Model (PRISM) at 4 km horizontal resolution [*Daly et al*., 2000]. An earlier study by *Scully* [2010] finds PRISM interpolated data to be a robust predictor of observed temperature records over the U.S.

2.4. Analyses

[20] We analyze three measures of snow-dominated water resources in the western U.S.:

[21] 1. *Percent change in 1 April snow water equivalent (SWE), November-December-January-February-March (NDJFM) precipitation, NDJFM snow-to-precipitation ratio, and NDJFM days with minimum temperature less than 0°C ("freeze days")*. For each variable, we first calculate the value in each year of the 1960–1999 and 2000–2039 periods. For each of these two 40 year time series, we then calculate the percentage departure from the baseline value (1960 for the 1960–1999 period, and the 1960–1999 mean for the 2000–2039 period) in each of the 40 years. We then fit a linear regression to each 40 year time series. Finally, we calculate the percent change as the percent difference between the last and first points on the regression line. (Note that this calculation of the percent change is insensitive to whether the time series of absolute magnitude or the time series of percent departure is used.)

[22] 2. *Partial correlation coefficients between 1 April SWE and NDJFM surface temperature and precipitation*. A partial correlation coefficient quantifies the correlation between the two variables when conditioning on other variables. In order to calculate the partial correlation between temperature and SWE, we first remove the effect of precipitation from temperature and SWE by linear regression, leaving two linear regression errors or residuals. We then calculate the partial correlation between temperature and SWE as the correlation between the two regression residuals [*de la Fuente et al*., 2004]. We repeat the same steps to calculate the partial correlation between precipitation and SWE by first removing the effect of temperature. At each grid point, we present partial correlations of precipitation and temperature with SWE in vector form, with precipitation as the x axis and temperature as the y axis. We calculate the orientation of each vector by taking the inverse tangent of the

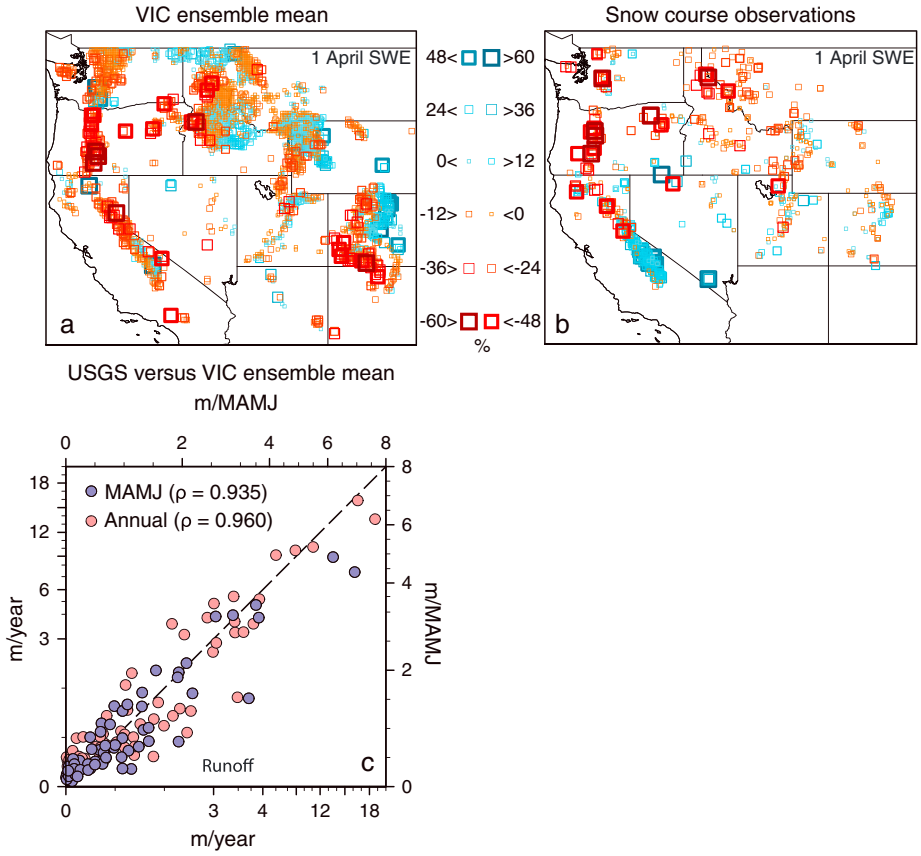

Figure 1. Comparison of VIC ensemble 1 April snow water equivalent (SWE) change and runoff mean with observations in 1960–1999 period. (a, b) 1 April SWE change in the VIC model simulation (Figure 1a) and snow course observations (Figure 1b). Changes are shown as percent change from the 1960 value. For both simulated and observed SWE, changes are only shown over those data points where average accumulated 1 April SWE in 1960–1999 is at least 10 mm, and only those observation sites with more than 35 years of data are used in analysis. (c) Comparison of simulated and observed 1960–1999 annual (red) and spring (March-April-May-June) (blue) runoff at 70 accounting units (HUC06) that contain snow course observations. The simulated runoff is calculated from the ensemble mean of the five VIC model simulations, with base flow and runoff summed directly for each HUC06 accounting unit without executing the separate routing model. The observed runoff is obtained from the U.S. Geological Survey (USGS) WaterWatch Computed Runoff. At a particular stream gauge location, runoff is computed by dividing the observed streamflow discharge by its corresponding drainage area. Further, observational runoff is aggregated to the HUC06 accounting units by calculating the weighted average of all stream gauges within each unit.

tangent ratio, which provides a measure of the SWE correlation with precipitation and temperature. We calculate future changes in these correlations by calculating the difference in the orientation of each vector in the 2000–2039 period with respect to its orientation in the 1960–1999 period.

[23] 3. *Changes in the date of the centroid of annual snowmelt, base flow, and runoff.* We analyze those HUC02 regions in the western U.S. for which snow course observations are available. We first calculate the grid point centroid date as the Julian day when 50% of the annual total occurs in each water year (1 October to 30 September [*Moore et al.*, 2007]). Using a kernel density function, we then calculate the probability density of centroid dates for the 1961–1999, 2000–2019, and 2020–2039 periods over the HUC02 regions. (For these water-year periods, the year designation corresponds with the year in which the water year ends; i.e., the 1961 water year begins 1 October 1960 and ends 30 September 1961.)

[24] We perform all analyses on the ensemble mean of the five VIC members by first calculating the mean time series at each grid point across the five VIC simulations. In addition, in order to probe the sensitivity of the results to internal climate system variability, we calculate the percent change in 1 April SWE and NDJFM precipitation, snow-to-precipitation ratio, and freeze days for each of the five VIC ensemble members. For all of the above measures, we consider only those grid points that exhibit 1 April SWE values of greater than or equal to 10 mm in the baseline period ensemble mean.

3. Results and Discussion

3.1. Ensemble Mean

[25] The VIC ensemble accurately represents the observed snow-dominated runoff across the western U.S., with a correlation of 0.96 (0.93) between simulated and observed annual

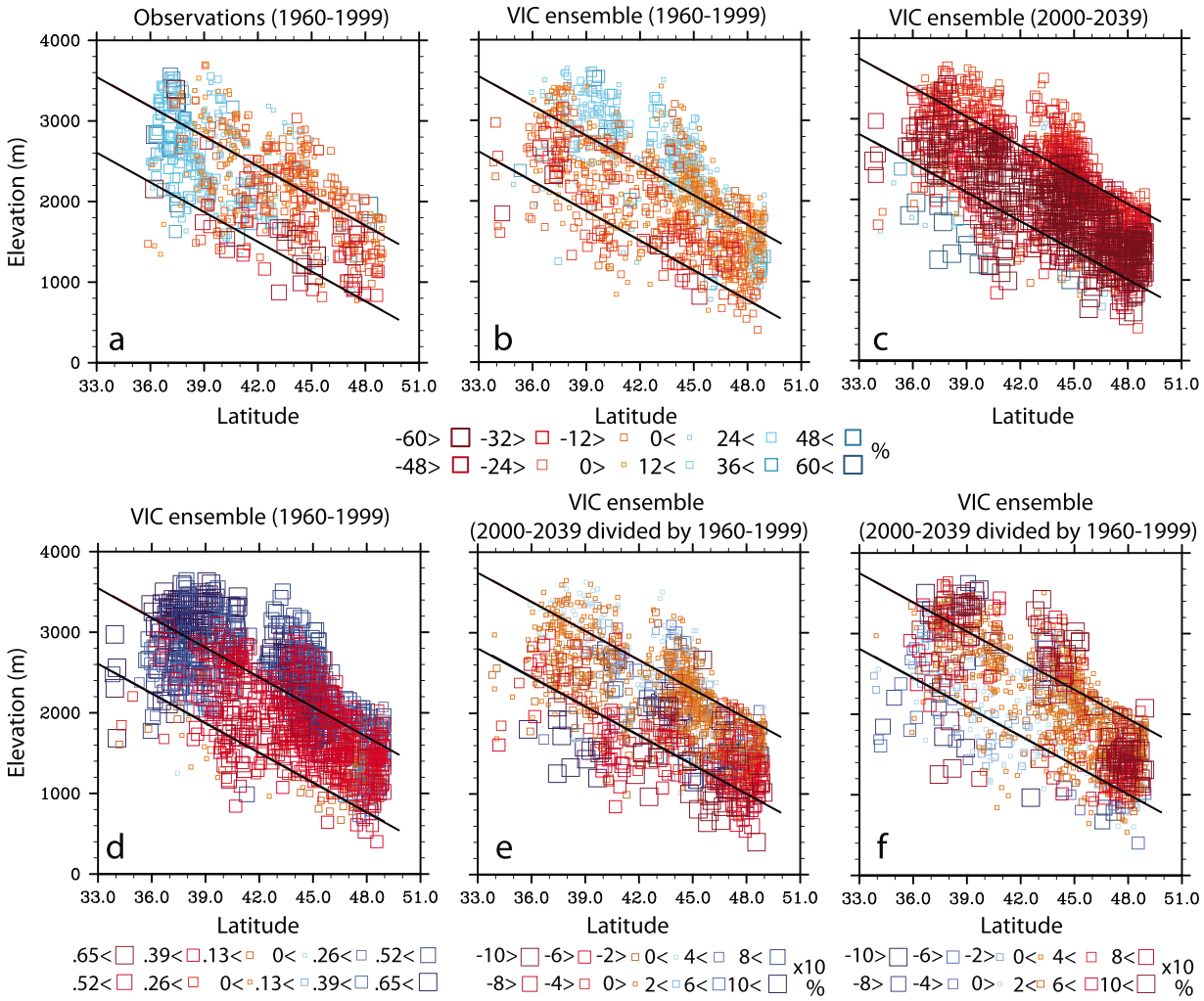

Figure 2. Change in 1 April SWE as a function of elevation and latitude. (a) Observational PRISM data (1960–1999). (b) VIC model ensemble mean in the baseline period (1960–1999). (c) VIC model ensemble mean in the future (2000–2039). Changes are calculated as percent change with respect to the baseline value (1960 for the 1960–1999 period, and the 1960–1999 mean for the 2000–2039 period). (d) Correlation of the dominant variable (precipitation or temperature) with 1 April SWE in VIC model ensemble in1960–1999. Blue colors represent grid points where correlation is higher with precipitation, and red colors represent the grid points where correlation is higher with temperature. (e) Percent change in the precipitation correlation with 1 April SWE in the future period with respect to the baseline period. (f) Percent change in the temperature correlation with 1 April SWE in the future period with respect to the baseline period. For ease of comparison, red colors in Figure 2e represent decrease in precipitation correlation, and red colors in Figure 2f represent increase in temperature correlation. The sloping lines in each panel represent the 0°C and −5°C isotherms. Isotherms are determined by the multiple linear regression of NDJFM temperature in 1960–1999 (Figures 2a, 2b, and 2d) and in 2000–2039 (Figures 2c, 2e, and 2f) on elevation and latitude. In the case of the observations, temperature isotherms are based on the PRISM data in 1960–1999. All panels show every other grid point.

(spring) runoff in the 70 HUC06 accounting units (Figure 1). The VIC ensemble also captures the regional pattern of late 20th century changes in 1 April SWE. For example, both the observations and the VIC model ensemble exhibit a predominance of decreasing 1 April SWE over more than 60% of the western U.S., along with a high concentration of strongly negative changes (stronger than −48%/40 years) over the moderately high elevations of northern California, Oregon, and Idaho (Figures 1 and 2). In addition, the VIC ensemble captures the observed regional relationships of SWE change with elevation and latitude (Figures 2a, 2b, and 3a) as well as the observed pattern of relatively high SWE correlation with temperature at lower elevations and relatively high SWE correlation with precipitation at higher elevations that is shown in *Mote* [2006] (Figure 2d). The most prominent area of disagreement between the simulated and observed changes in 1 April SWE occurs in California over the southern Sierra Nevada, with the observations showing primarily increasing trends and the VIC ensemble showing primarily decreasing trends (Figures 1 and 2). Despite these

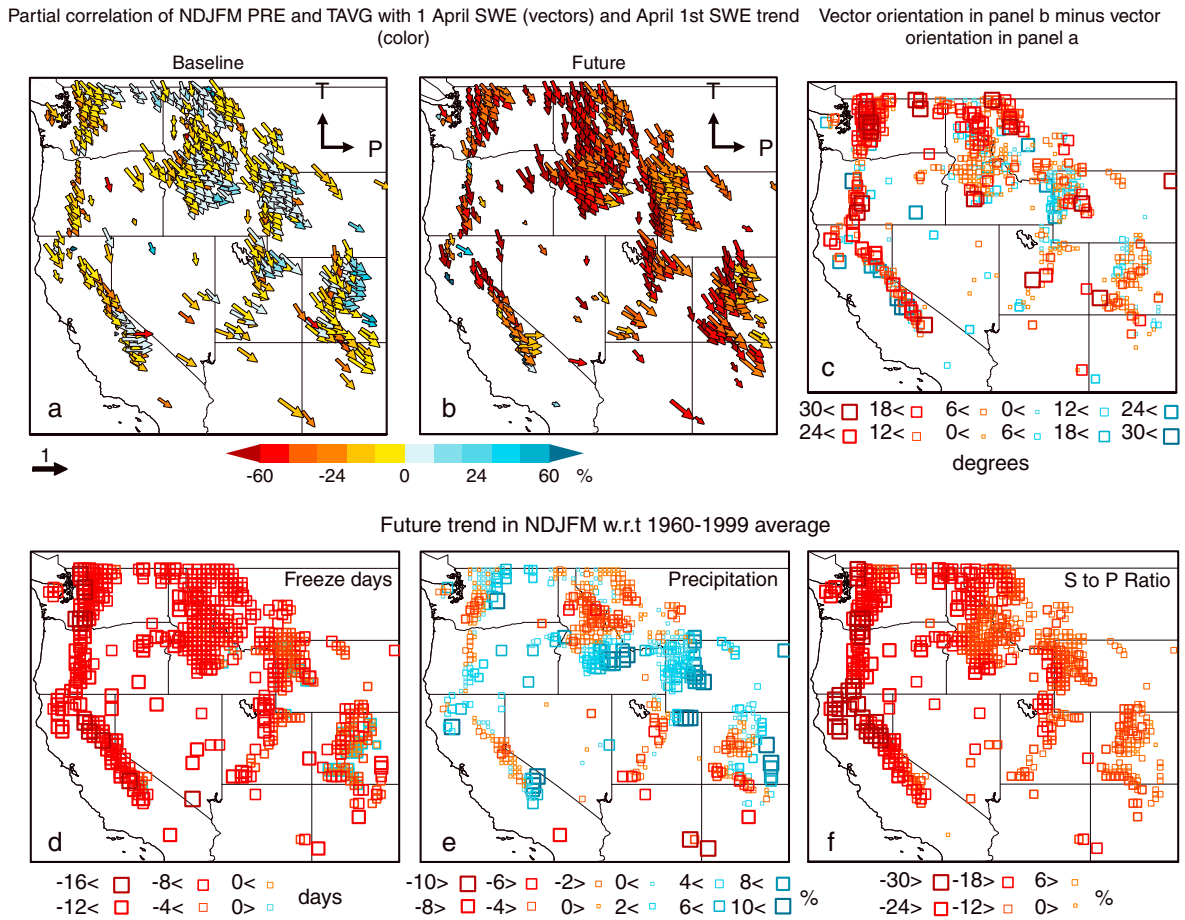

Figure 3. Changes in snow, precipitation, and temperature. (a, b) Partial correlation of cold-season averaged daily precipitation and mean daily temperature with 1 April snow water equivalent (SWE). Vectors represent the partial correlation of November-December-January-February-March (NDJFM) temperature and precipitation with 1 April SWE in 1960–1999 (Figure 3a) and 2000–2039 (Figure 3b). The vectors are oriented with precipitation as the *x* axis and temperature as the *y* axis, meaning that a vector oriented toward the southeast is correlated positively with precipitation and negatively with temperature. Magnitude of each vector represents the partial correlation with the dominant variable. The colors show the SWE percent change with respect to the baseline value (1960 for the 1960–1999 period, and the 1960–1999 mean for the 2000–2039 period). (c) The change in the relationship of 1 April SWE with NDJFM precipitation and temperature in the future period. We calculate future changes in these relationships by calculating the difference in the orientation of each vector in Figure 3b with respect to its orientation in Figure 3a. Blue colors represent increase in correlation with precipitation, and red colors represent increase in correlation with temperature. (d, e, f) Changes in NDJFM days with minimum temperature below 0°C, NDJFM precipitation, and NDJFM snow-to-precipitation ratio (respectively). All panels show every other grid point.

differences, the VIC ensemble shows greater agreement with observed historical 1 April SWE trends than the corresponding GCM-VIC ensemble, the latter of which shows greater mismatch with the observations over parts of the Rocky Mountains and exacerbated bias over Sierra Nevada region (Figures 1 and 4a). (It should also be noted that the observations represent only one realization of the coupled climate system, meaning that differences in local or regional trends between the ensemble and observations could be due to physical errors in the modeling system or to arbitrary differences in phasing of variability; see discussion of the individual realizations below.)

[26] In contrast to the 1960–1999 period, almost all points in the VIC ensemble exhibit a negative trend in 1 April SWE over the 2000–2039 period, with most points exhibiting a negative trend that is stronger than −30%/40 years (Figures 2c and 3b). SWE changes are also substantially larger in magnitude over the 2000–2039 period than over the 1960–1999 period (Figures 2c and 3b), implying an acceleration of the decrease in spring snowpack over the near-term decades (Hereafter, the term acceleration is used to describe situations in which the rate of change over 40 years in the future period is greater than the rate of the change over 40 years in the baseline period). This near-term acceleration is consistent with the trends in regional cold-season temperature, with all five HUC02 regions exhibiting a rate of NDJFM warming that is at least three times as large over the 2000–2039 period as over the 1960–1999 period (Figure 5). SWE changes in the 2000–2039 period are generally more strongly negative at points corresponding to elevations

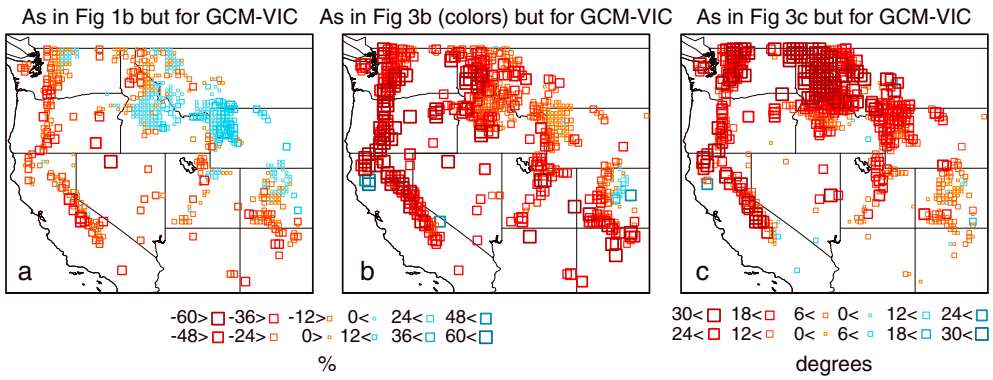

Figure 4. Percent change in 1 April SWE with respect to the baseline value (1960 for the 1960–1999 period, and the 1960–1999 mean for the 2000–2039 period) in the ensemble mean of the GCM-VIC in (a) baseline (1960–1999) and (b) future (2000–2039) periods. Figure 4a can be compared with Figures 1a and 1b, and Figure 4b can be compared with Figure 3b where colors represent 1 April SWE trend in future period. (c) The change in the relationship of 1 April SWE with NDJFM precipitation and temperature in the future period. The calculation of changes in SWE relationship with NDJFM precipitation and temperature is consistent with the methodology described in Figure 3c.

between the 0°C and −5°C isotherms than at points corresponding to elevations higher than the −5°C isotherm, meaning that for a given latitude, changes are generally more negative at low elevations than at high elevations (Figure 2c). (We calculate the isotherm elevation by multiple linear regression of NDJFM temperature on elevation and latitude, as described in *Mote* [2006].) However, while the majority of points that correspond to the elevations higher than the −5°C isotherm exhibit positive SWE changes in the 1960–1999 period, almost all points that correspond to the elevations higher than the −5°C isotherm exhibit negative SWE changes in the 2000–2039 period. Further, both the 0°C isotherm and the −5°C isotherm are found approximately 200 m higher in elevation in the future period than in the baseline period (Figure 2c).

[27] Declines in 1 April SWE could result from decreases in cold-season precipitation, decreases in the snow-to-precipitation ratio, increases in the snow sublimation prior to 1 April, and/or increases in the snowmelt prior to 1 April. Moreover, even with increases in cold-season precipitation, decreases in 1 April SWE can still occur if increasing cold-season temperatures lead to decreases in freeze days, thereby leading to (1) more precipitation falling as rain rather than snow and a decrease in snow-to-precipitation ratio, and/or (2) faster rate of snowmelt during the cold season and greater loss of accumulated snow prior to 1 April. In our analysis of the VIC ensemble simulations for the 2000–2039 period, the snow-to-precipitation ratio shows a decrease of up to >30%/40 years across the western U.S (Figure 3f), favoring a decline in 1 April SWE. Further, many regions with negative changes in 1 April SWE (up to >60%/40 years) and snow-to-precipitation ratio (up to >30%/40 years) exhibit positive changes in precipitation (up to >10%/40 years), including parts of the Pacific Northwest, Rocky Mountains, and Sierra Nevada (Figure 3e). Moreover, even over the regions with negative precipitation change, the decline in snow-to-precipitation ratio and 1 April SWE is much stronger (up to >30%/40 years) than the decrease in the amount of precipitation (up to 6%/40 years).

[28] It should be noted that with no change in snow-to-precipitation ratio and no change in cold-season snowmelt, a 30% decrease in 1 April SWE accumulation requires a 30% decrease in precipitation. The fact that 1 April SWE and NDJFM snow-to-precipitation ratio both show substantially larger 2000–2039 trends than NDJFM precipitation suggests that precipitation change is not the dominant driver of the simulated near-term changes in snow hydrology over the western U.S. Rather, we find increased influence of temperature on SWE, with most areas showing a greater correlation of SWE with temperature in the 2000–2039 period than in the 1960–1999 period (Figure 3c), consistent with previous studies of the observed 20th century changes in snow hydrology [e.g., *Hamlet et al.*, 2005; *Bonfils et al.*, 2008] as well as modeling studies of the projected 21st century SWE responses to increase in radiative forcing [e.g., *Christensen and Lettenmaier*, 2007]. The largest increases in temperature influence are concentrated over the Sierra Nevada in California and the Cascades in the Pacific Northwest, as well as the northern Rocky Mountains in Idaho and Montana. The strongest increase in temperature influence is seen primarily at points corresponding to elevations between the 0°C and −5°C isotherms south of 40°N (which also have shown relatively high sensitivity to historical warming; Figure 2a [*Das et al.*, 2009; *Mote*, 2006]), and at points corresponding to elevations higher than the baseline −5°C isotherm north of 45°N (Figure 2e and 2f).

[29] This shift toward increased temperature influence suggests that continued regional warming like that projected for the near-term period causes the variability of 1 April SWE to be driven less by variations in the amount of moisture that is delivered during the season and more by the amount of time spent above freezing during the season. In particular, the shift toward increased temperature influence is associated with negative changes in the number of NDJFM freeze days (Figure 3d), and the changes in NDJFM freeze days exhibit a correlation of −0.72 with changes in NDJFM snow-to precipitation ratio. The decrease in NDJFM freeze days also helps to explain the strong changes in the snow hydrology over the elevations higher than the −5°C isotherm, where mean cold-season temperatures in the future period are still

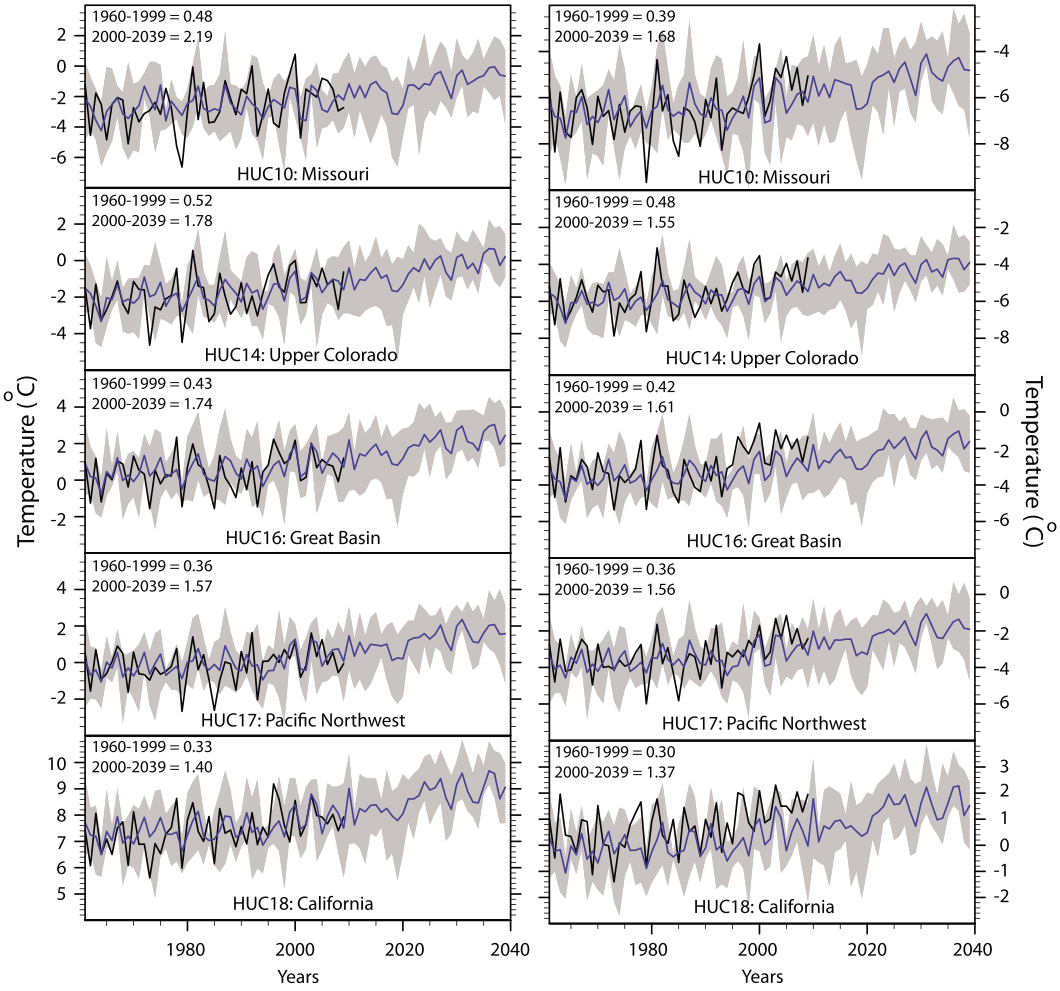

Figure 5. NDJFM average temperature calculated over the HUC02 regions. The VIC model ensemble mean is shown in blue, and the VIC model ensemble range is shown in grey. The observational PRISM values are shown in black. (left column) The mean values over all grid points in each HUC02 region. (right column) The mean values over the grid points with 1 April SWE greater than 10 mm in each HUC02 region. The slope (per 40 years) is also shown for each region.

below 0°C but where snow-to-precipitation ratio and accumulated 1 April SWE show a decline because of the fewer days with temperatures below freezing.

[30] Given previous results suggesting that fine-scale climate processes—such as topographically controlled snow-albedo feedbacks—amplify the magnitude of cold-season warming that occurs in response to high greenhouse gas concentrations [*Rauscher et al.*, 2008], we test whether the low- and high-resolution climate models in our modeling system produce different changes in SWE over the near-term decades. Interestingly, while the GCM-VIC ensemble exhibits differences from the VIC ensemble in the simulation of the sign of baseline 1 April SWE trends, it simulates strong decreases in the projected 1 April SWE across the western U.S. consistent with the VIC ensemble trends. This agreement in the future responses between the VIC and GCM-VIC ensembles results primarily from the fact that increasing temperature influence accelerates 1 April SWE decline in both ensembles (Figures 3 and 4). Whether the magnitude of SWE trend remains similar between the VIC and GCM-VIC ensembles at higher levels of forcing (such as in the late 21st century of the A1B scenario) requires additional modeling experiments. Likewise, whether the magnitude of SWE trend is similar on smaller spatial scales (such as within an individual basin) requires further analysis, although we note that bias correction (such as employed in our experiments) can substantially reduce the spread in simulated climate change impact between low- and high-resolution climate models by reducing the intermodel spread in the proximity to critical impacts thresholds in the baseline period [*Diffenbaugh and Scherer*, 2013].

[31] In addition to decreasing the natural reservoir of water available in snowpack at the end of the cold season, near-term warming also alters the hydrologic timing throughout the western U.S. (Figure 6). The shift in hydrologic timing is more pronounced in the later half of the near-term period, with all regions exhibiting earlier central dates of snowmelt, runoff, and base flow in the 2020–2039 period than in the 2000–2019 period. This acceleration in hydrologic response in the 2020–2039 period can be traced to the fact that regional temperature changes are also relatively stronger in the 2020–2039 period (Figure 5). The changes in hydrologic timing in the 2020–2039 period

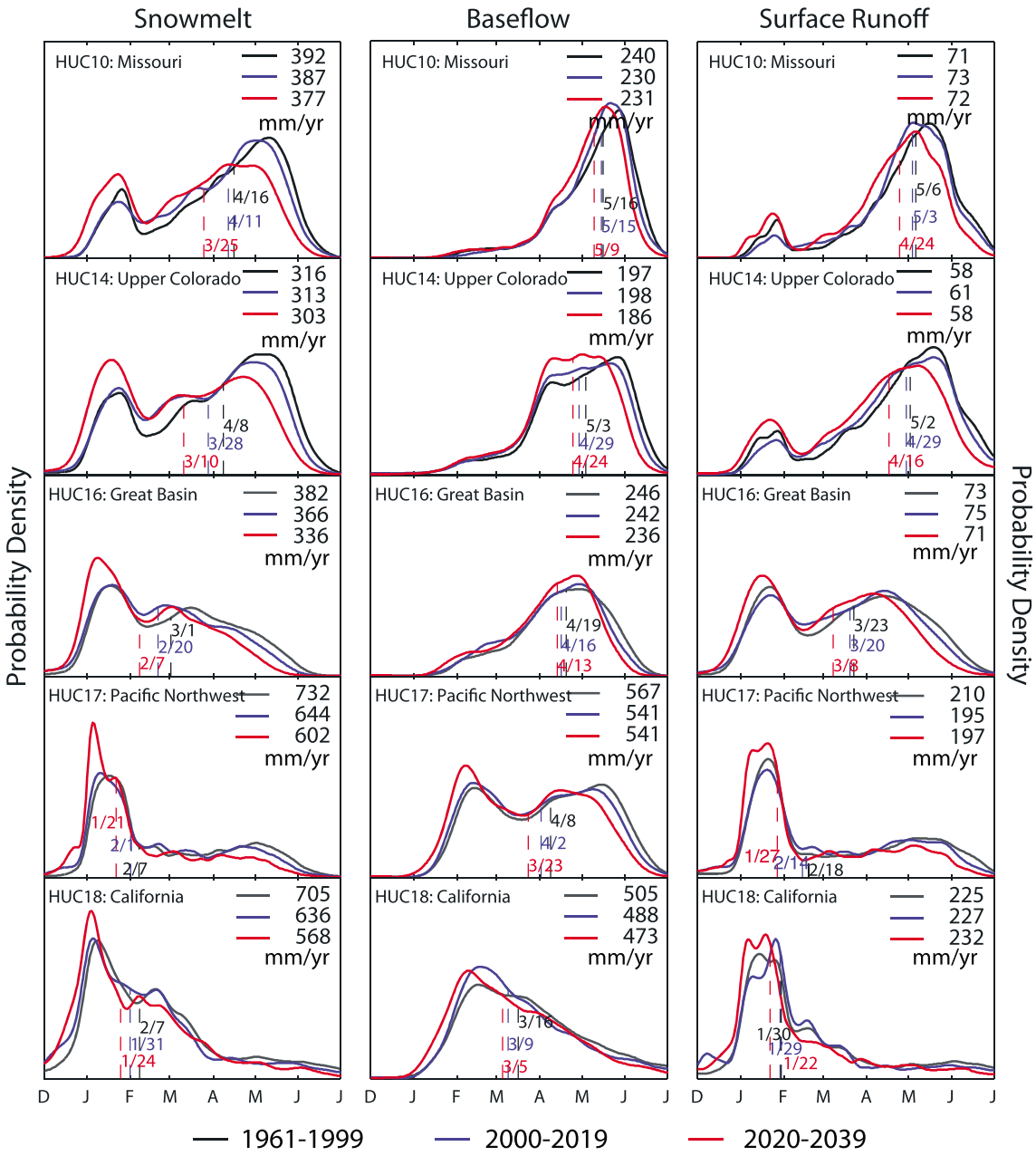

Figure 6. VIC ensemble date of the centroid of annual snowmelt, base flow, and runoff for hydrologic regions (HUC02) in the western U.S., calculated as the date at which 50% of water-year (1 October to 30 September) total has occurred. The calculation is done in each water year for each ensemble member over the grid points with 1 April SWE values of greater than or equal to 10 mm in the 1960–1999 period. The probability densities of central dates are estimated using kernel density functions for the 1961–1999 (black), 2000–2019 (blue), and 2020–2039 (red) periods. The mean annual amount (mm/yr) is also calculated for each period.

include shifts as large as 4 weeks for snowmelt (Upper Colorado), 2 weeks for base flow (Pacific Northwest), and 4 weeks for runoff (Pacific Northwest). All HUC02 regions exhibit a greater shift in central snowmelt date than in central base flow date or surface runoff date. In addition, the total annual snowmelt and base flow are reduced in the 2020–2039 period (relative to the 1960–1999 period) in all regions. Further, while the total annual surface runoff is reduced in only the Great Basin and Pacific Northwest regions, the total surface runoff after 1 May is reduced in all regions, while the total surface runoff prior to 1 February is increased in all regions. The projected changes in surface runoff in the western U.S. are consistent with the earlier findings that show a strong sensitivity of surface runoff to the increase in surface warming [*Das et al.*, 2011; *Vano et al.*, 2012].

[32] Taken together, these simulated changes in snow hydrology suggest a transition to a substantially more liquid-dominated water resources regime in the western U.S. over the near-term decades.

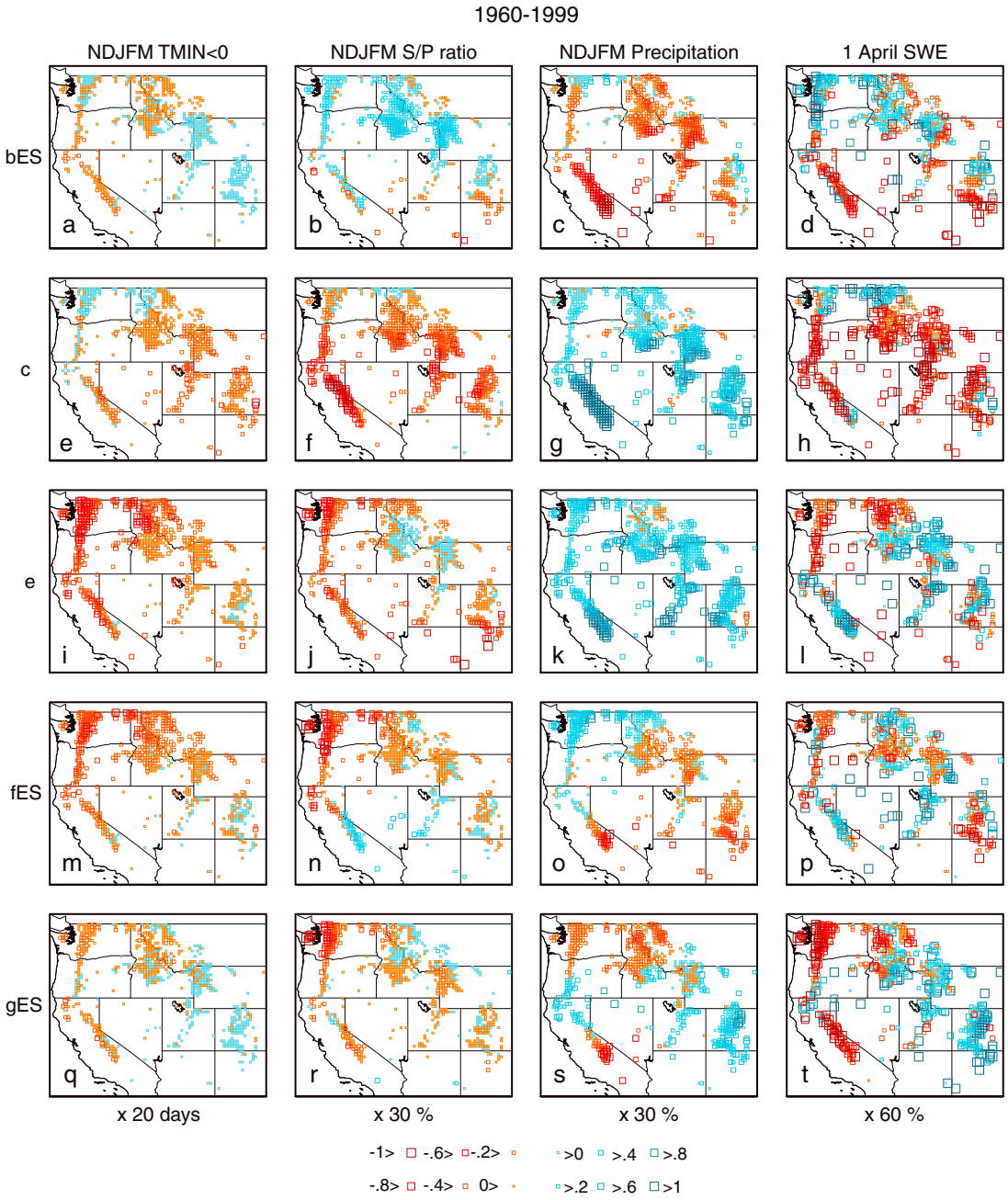

Figure 7. Baseline (1960–1999) trends per 40 years in November-December-January-February-March (NDJFM) number of freeze days, snow-to-precipitation ratio, and precipitation, and 1 April SWE in individual ensemble members. (a–d) bES, (e–h) c, (i–l) e, (m–p) fES, and (q–t) gES. Trends are calculated with respect to the 1960 value over the grid points where ensemble mean baseline 1 April SWE is greater than 10 mm. All panels show every other grid point.

3.2. Uncertainty in Near-Term Climate Change

[33] The fact that the changes in SWE are associated with increased correlations with temperature and decreased correlations with precipitation suggests that changes in snow-related water resources cannot be reliably projected over the near-term decades by simply applying the historical correlations to projected changes in temperature and precipitation. In addition, the fact that the projected hydrologic changes are strongly associated with changes in temperature should increase confidence in the results [*Barnett et al.*, 2005], as projected near-term changes in regional temperature are far more robust than projected near-term changes in regional precipitation [*Hawkins and Sutton*, 2010]. However, the evolution of regional climate on decadal time scales presents a particularly difficult scientific challenge [e.g., *Cane*, 2010], creating substantial uncertainty in near-term regional climate change [e.g., *Hawkins and Sutton*, 2010], particularly in snow-dominated regions [e.g., *Stewart*, 2009].

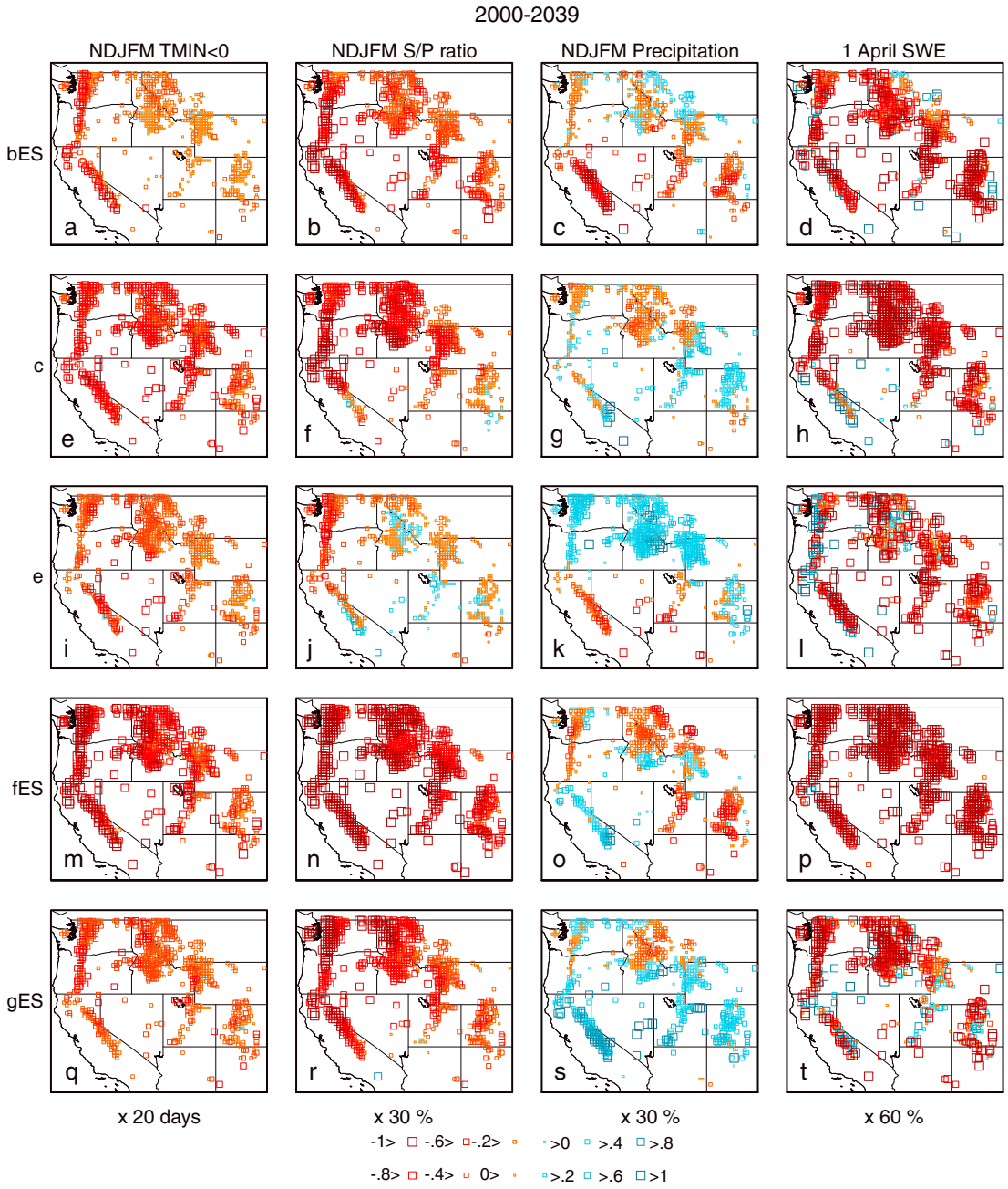

Figure 8. Future (2000–2039) trends per 40 years in November-December-January-February-March (NDJFM) number of freeze days, snow-to-precipitation ratio, and precipitation, and 1 April SWE in individual ensemble members. (a–d) bES, (e–h) c, (i–l) e, (m–p) fES, (q–t) gES. Trends are calculated with respect to the 1960–1999 average value over the grid points where ensemble mean baseline 1 April SWE is greater than 10 mm. All panels show every other grid point.

[34] In order to probe this uncertainty, we compare the individual realizations in the five-member ensemble. In doing so, we find that the five ensemble members exhibit substantial variation in the pattern of hydroclimatic trends over the 1960–1999 period (Figure 7). For example, the disagreement in 1 April SWE seen in the ensemble mean over the southern Sierra (including high elevations south of 39°N) and areas of the Rockies (including high elevations between 42°N and 45°N) is not seen uniformly across the individual ensemble members, with two of the five members showing increasing trends over the southern Sierra (Figures 7l and 7p) and two of the five ensemble members showing decreasing trend between 42 N and 45 N (Figures 7h and 7p), in agreement with observations. Additionally, one of the five VIC ensemble members closely captures the pattern of observed trend in 1 April SWE throughout the western U.S. (Figures 1b and 7p). Indeed, no subregion of the western U.S. exhibits a consistent sign of the 1960–1999 trends in NDJFM snow-to-precipitation ratio, NDJFM precipitation, or 1 April SWE across the five-member ensemble, highlighting the

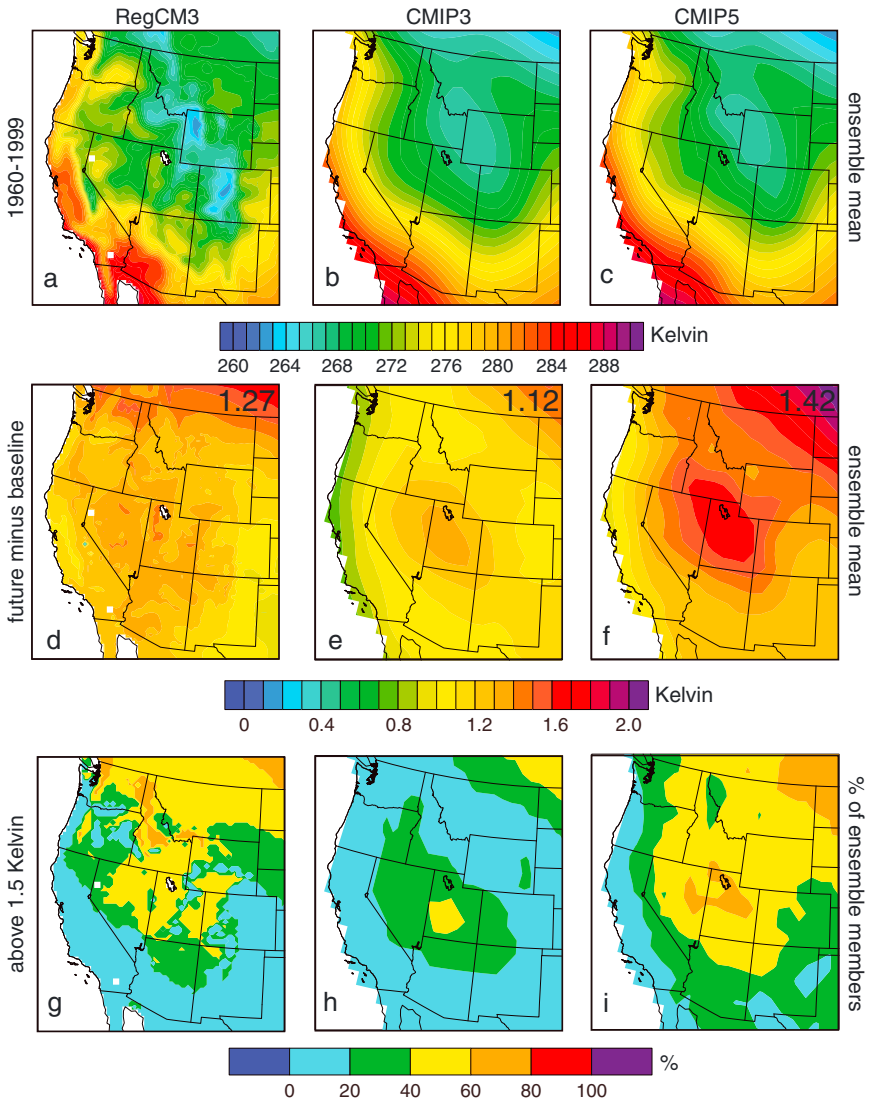

Figure 9. Comparison of RegCM3 ensemble with CMIP3 and CMIP5 ensembles. Ensemble mean NDJFM temperature (K) for the 1960–1999 period calculated in (a) RegCM3, (b) CMIP3, and (c) CMIP5. Ensemble mean changes (2006–2039 minus 1960–1999) in mean NDJFM temperature (K) calculated in (d) RegCM3, (e) CMIP3, and (f) CMIP5. The numbers in Figures 9d, 9e, and 9f represent domain averaged values. Percent of the ensemble members showing warming greater than 1.5 K in the mean NDJFM temperature (K) in (g) RegCM3, (h) CMIP3, and (i) CMIP5.

important influence of internal climate system variability over the late 20th century.

[35] In contrast, we find that the 2000–2039 changes seen in the ensemble mean are robust across all the individual ensemble members (Figure 8, rightmost column). For example, although the individual realizations exhibit varying signs in 1 April SWE trends over the 1960–1999 period (Figure 7, rightmost column), they exhibit consistently negative 1 April SWE trends over the 2000–2039 period (Figure 8, rightmost column), strengthening the conclusion of accelerating decrease in spring snowpack in the near-term decades. In addition, we find that, in most areas, the 2000–2039 trend in 1 April SWE in the individual ensemble members is not driven by the 2000–2039 trend in precipitation, with most members exhibiting negative 2000–2039 trends in 1 April SWE despite substantial variations in the sign of 2000–2039 trends in precipitation (Figure 8, right two columns). Further, the negative 2000–2039 trends in cold-season precipitation in the individual ensemble members are mostly weak compared to the corresponding 2000–2039 trends in 1 April SWE. That many areas in the individual ensemble members exhibit positive 2000–2039 trends in cold-season precipitation coupled with negative trends in 1 April SWE and that the negative trends in 1 April SWE are generally much stronger than the corresponding negative trends in cold-season precipitation strengthens the conclusion that the negative 2000–2039 trends in 1 April SWE are driven primarily by temperature.

[36] In addition, although the individual realizations exhibit varying signs in trends in cold-season freeze days and snow-to-precipitation ratio over the 1960–1999 period (Figure 7, left two columns), they exhibit consistently negative trends in cold-season freeze days and snow-to-precipitation ratio over the 2000–2039 period (Figure 8, left two columns). Therefore, as with SWE, the changes in cold-season freeze days and

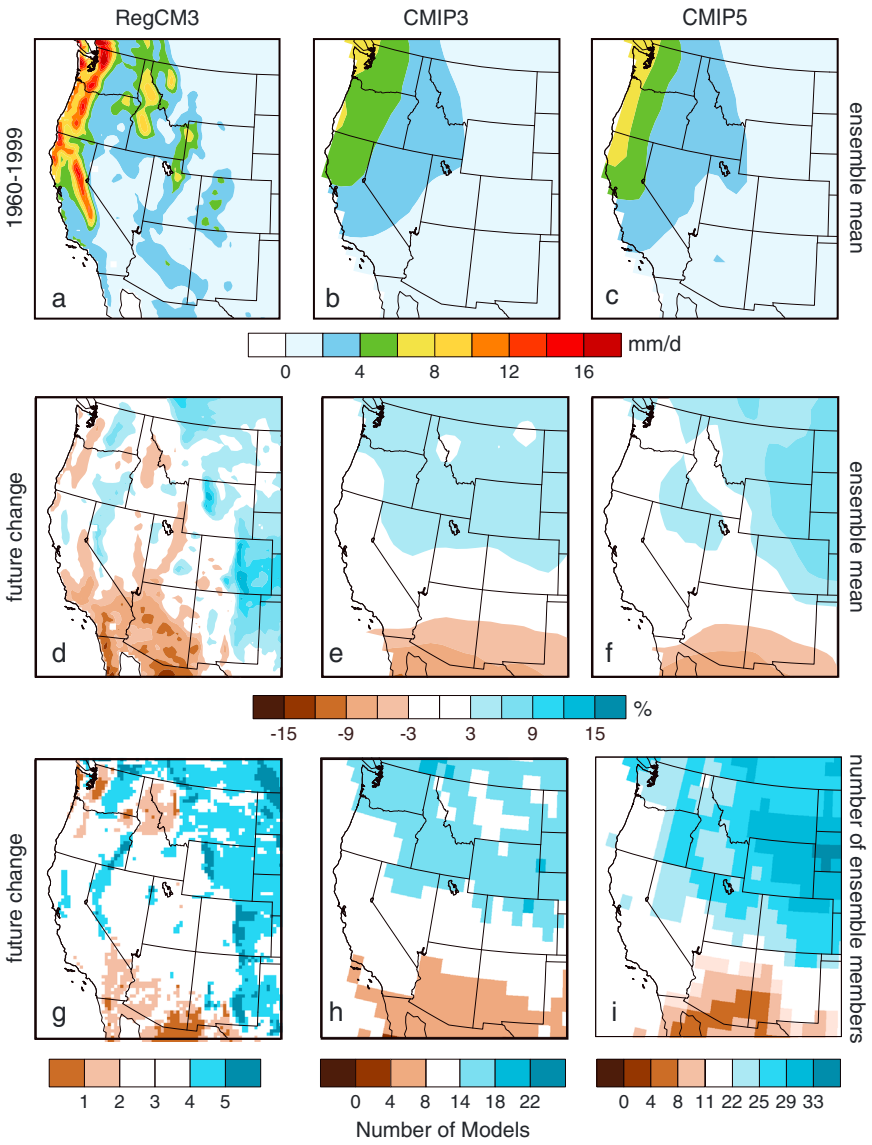

Figure 10. Comparison of RegCM3 ensemble with CMIP3 and CMIP5 ensembles. Ensemble mean NDJFM precipitation (mm/day) for the 1960–1999 period calculated in (a) RegCM3, (b) CMIP3, and (c) CMIP5. Ensemble mean percent change (2006–2039 divided by 1960–1999) in mean NDJFM precipitation (%) calculated in (d) RegCM3, (e) CMIP3, and (f) CMIP5. Number of the ensemble members that simulate an increase in precipitation (g) RegCM3, (h) CMIP3, and (i) CMIP5. Blue (brown) color represents the regions where more than two thirds of the GCMs simulate an increase (decrease) in precipitation. White regions are where simulated precipitation response is uncertain.

snow-to-precipitation ratio that are seen in the ensemble mean (Figures 3d and 3f) are also robust across the individual ensemble members (Figure 8, left two columns). Further, the spatial correlation between the trends in cold-season freeze days and snow-to-precipitation ratio increases from 0.58 in the 1960–1999 period to 0.70 in the 2000–2039 period, with the strongest decreases in snow-to-precipitation ratio (~ −30%) and number of freeze days (~ −20 days) both occurring over the Pacific Northwest and California regions. That the individual members exhibit a clear transition to consistent trends not only in 1 April SWE but also in cold-season freeze days and snow-to-precipitation ratio during the 2000–2039 period strengthens the conclusion of an accelerating transition to more liquid-dominated water resources.

[37] The above comparisons of the individual realizations of our CCSM3-RegCM3-VIC single-model ensemble help to constrain the uncertainty arising from internal climate system variability. However, our modeling system represents just one of many different representations of the climate system, and it is impossible to know a priori which construction is correct. This uncertainty in climate model structure creates additional uncertainty beyond that arising from internal climate system variability [e.g., *Hawkins and Sutton*, 2010]. Ideally, we could compare these sources of uncertainty (and that arising from uncertainty in climate forcing pathway) through a suite of experiments consisting of multiple realizations of multiple GCM-RCM (Regional Climate Model) hydrologic model combinations. Unfortunately, the limited availability of

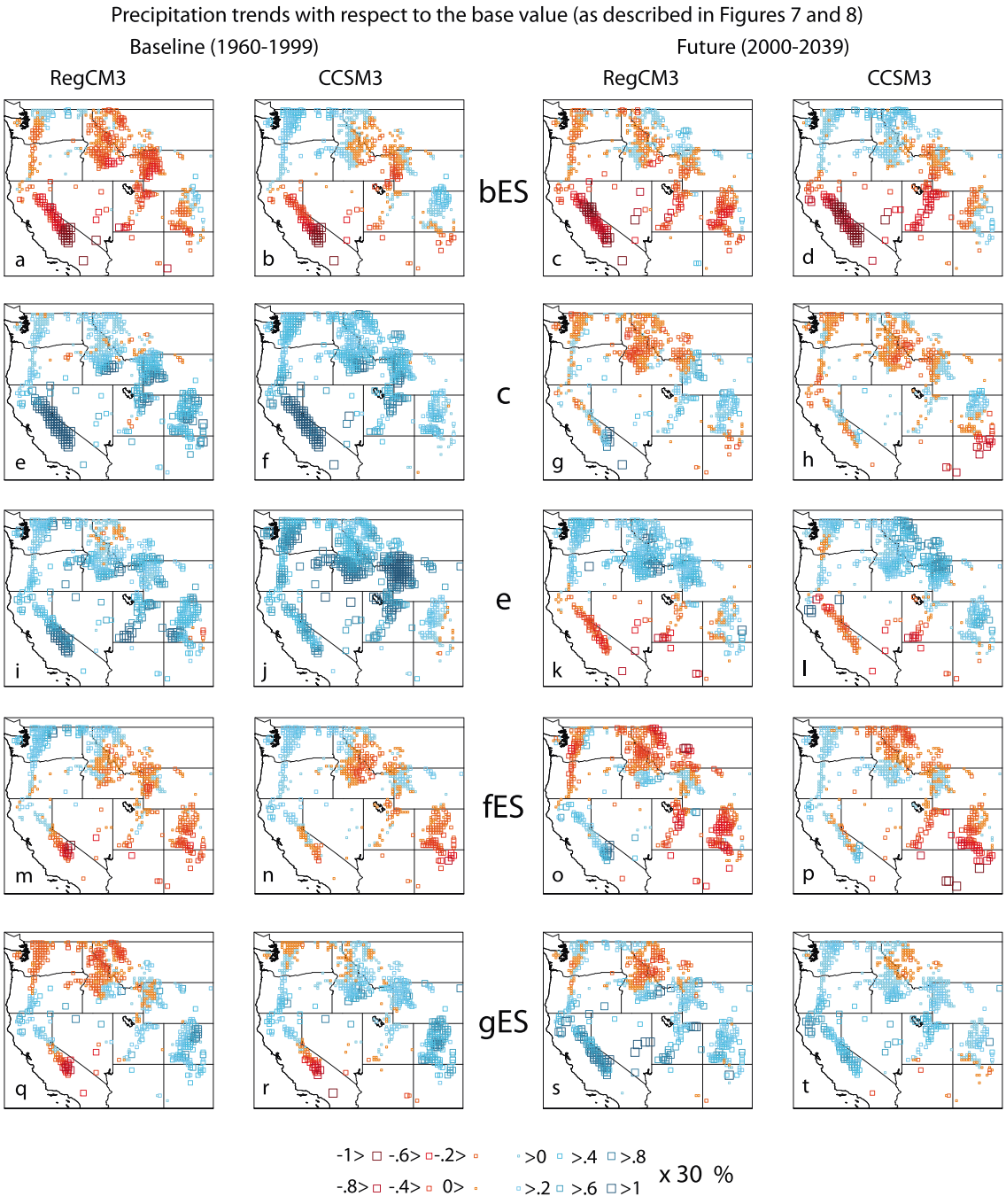

Figure 11. Comparison of trends per 40 years (as described in Figures 7 and 8) in November-December-January-February-March (NDJFM) precipitation in the corresponding individual ensemble members of CCSM3 and RegCM3. (leftmost column) RegCM3 baseline, (second column from left) CCSM3 baseline, (second column from right) RegCM3 future, and (rightmost column) CCSM3 future.

projections of daily-scale temperature and precipitation for the near-term period [*Mearns et al.*, 2009; *Meehl et al.*, 2007a] limits our analysis to one GCM-RCM configuration. However, we are able to probe the model uncertainty domain by comparing the seasonal-scale temperature and precipitation changes seen in our high-resolution ensemble with those seen in the CMIP3 and CMIP5 multi-GCM ensembles.

[38] We note that the ensemble means of cold-season precipitation and temperature in the baseline period (Figures 9b, 9c, 10b, and 10c) and the projected precipitation changes in the future period (Figures 10e and 10f) are quite similar between the CMIP3 and CMIP5 ensembles. However, the magnitude of cold-season temperature change is stronger in the CMIP5 RCP8.5 ensemble than in the CMIP3 SRES A1B ensemble (Figures 9e and 9f). This stronger temperature response in CMIP5 is partly attributable to the fact that the future CO_2 concentrations in RCP8.5 are higher than those in SRES A1B in the 2030s [*Peters et al.*, 2013]. Further, in order to probe the characteristics of the temperature response in the individual ensemble members,

we also show the percent of the individual ensemble members that simulate a temperature increase of at least 1.5 K. As with the mean temperature changes, the percent of GCMs with a temperature increase of 1.5 K or more is twice as large in the CMIP5 RCP8.5 ensemble as in the CMIP3 SRES A1B ensemble (Figures 9h and 9i), meaning that the stronger temperature response is largely consistent across the GCMs in the CMIP5 RCP8.5 ensemble. Moreover, the GCMs in the CMIP3 and CMIP5 ensembles show little intermodel agreement in the sign of precipitation response along most of the West Coast, where precipitation changes are mostly less than 3% of the baseline mean (Figures 10h and 10i).

[39] Cold-season precipitation and temperature changes generally show stronger spatial variability in our high-resolution RegCM3 ensemble (Figures 9d and 10d). We note that the mean temperature changes in the RegCM3 ensemble are comparable to those in the CMIP3 ensemble (with the exception of the changes along the coast) and are less than those in the CMIP5 ensemble. However, the percent of the ensemble members showing warming of at least 1.5 K in the RegCM3 ensemble is comparable to that in the CMIP5 ensemble across most of the western U.S. (Figure 9g). Moreover, the mean precipitation changes in RegCM3 ensemble are generally slightly larger than the corresponding changes in the CMIP3 and CMIP5 ensembles. While stronger heterogeneity of the cold-season temperature and precipitation responses in our high-resolution RegCM3 ensemble can be attributed to the realistic representation of their spatial variability compared to the coarse resolution CMIP3 and CMIP5 ensembles (Figures 9a–9c and 10a–10c), stronger precipitation changes are also consistent with the precipitation response in the driving CCSM3 simulations (Figure 11).

[40] However, it is important to note that existing multimodel ensembles are likely too small to distinguish the effects of model structure from the effects of internal climate system variability. In particular, the recent 40-member single-model ensemble experiment of *Deser et al*. [2012] shows that the uncertainty in the cold-season precipitation trend arising from internal atmospheric variability can be as large as that seen in single-member multimodel ensembles such as we show in CMIP3 and CMIP5 (Figure 10). This pronounced single-model spread seen in *Deser et al*. [2012] suggests that the spread between the different CMIP models could largely be due to internal climate system variability rather than differences in model construction. At a minimum, the single-model spread suggests that considerably larger ensembles of each model are needed in order to distinguish uncertainty in model construction from uncertainty in internal variability.

[41] The single-model spread seen in the large ensemble of *Deser et al*. [2012] also highlights the fact that the real evolution of the climate system over recent decades has been only one realization of a noisy system. The fact that only one of the five realizations in our VIC ensemble closely matches the pattern of observed trend throughout the western U.S. (Figures 1b and 7p) suggests that in the recent forcing regime, internal climate system variability could create increasing trends in 1 April SWE in some areas, even within the context of global warming. Further, the fact that the VIC ensemble shows acceleration of decreasing 1 April SWE in the near-term decades in realizations with increasing near-term precipitation trends and realizations with decreasing near-term precipitation trends (Figure 8) suggests that near-term warming could overwhelm uncertainty in the sign of near-term precipitation trends over that region.

[42] It should also be noted that although 1 April SWE is an important indicator of snow accumulation and water availability in the region [*Bohr and Aguado*, 2001; *Kapnick and Hall*, 2012; *Mote et al*., 2005], different snow-related measures could show different responses to continued global warming [*Pierce and Cayan*, 2013].

4. Conclusions

[43] Our high-resolution ensemble experiment improves the quantification of future changes in snow-dominated water resources in the western U.S. over the 2000–2039 period. Simulations of the recent past are in general agreement with observations, except in places where winter precipitation varies substantially over the period of analysis.

[44] The projected near-term hydrologic changes are substantial, even though the simulated global warming is only approximately 1°C above the 20th century baseline [*Meehl et al*., 2006]. An important result of this research is that the trends in hydrologic variables in the 2000–2039 period are substantially larger and more robust than in the 1960–1999 period, suggesting an accelerating emergence of hydrologic change in the near-term decades as the response to global warming emerges more robustly from the noise of internal climate system variability.

[45] These projected hydrologic changes could have important impacts on natural and human systems. For example, increases in wildfire activity and vulnerability of riparian ecosystems in western North America have both been linked to observed trends toward earlier spring snowmelt [e.g., *Rood et al*., 2008; *Westerling et al*., 2006], suggesting that the near-term shifts in snowmelt projected by our high-resolution ensemble could further exacerbate these risks. Forest die-off in the western U.S. has likewise been linked to drought and associated pest infestation [e.g., *Adams et al*., 2009; *Allen et al*., 2010; *Breshears et al*., 2005; *Park Williams et al*., 2013], suggesting that the projected near-term decrease in warm-season runoff could also increase stress on terrestrial ecosystems. Further, given the dependence of the regional water management system on snowpack and snowmelt, the projected near-term increases in runoff in the winter and decreases in the spring and summer—which are associated with increasing winter snowmelt and decreasing snow-to-precipitation ratio—can be expected to increase the need for capacity to capture liquid water in the winter and store it through the summer. While specific management decisions should be taken with caution, our results suggest an accelerating need for systems to cope with liquid-dominated water resources over the near-term decades.

[46] **Acknowledgments.** We thank two editors and five anonymous reviewers for their insightful and constructive comments through five submissions over the past two years. We thank the Rosen Center for Advanced Computing (RCAC) at Purdue University for access to computing resources. We thank the modeling groups, the WCRP's WGCM, PCMDI, and the U.S. DOE for enabling the CMIP3 and CMIP5 archives, the North American Regional Climate Change Assessment Program for the NARCCAP archive, the Oregon State University for PRISM data, and the USGS for WaterWatch data. This work was supported by NSF award 0955283; DOE awards 3ERKP777, DE-FG02-08ER64649, and DE-SC0001483; and ORNL LDRD award 32112413.

References

Adam, J. C., A. F. Hamlet, and D. P. Lettenmaier (2009), Implications of global climate change for snowmelt hydrology in the 21st century, *Hydrol. Processes*, *23*(7), 962–972.

Adams, H. D., M. Guardiola-Claramonte, G. A. Barron-Gafford, J. C. Villegas, D. D. Breshears, C. B. Zou, P. A. Troch, and T. E. Huxman (2009), Temperature sensitivity of drought-induced tree mortality portends increased regional die-off under global-change-type drought, *Proc. Natl. Acad. Sci. U. S. A.*, *106*(17), 7063–7066.

Aguado, E., D. Cayan, L. Riddle, and M. Roos (1992), Climatic fluctuations and the timing of west-coast streamflow, *J. Clim.*, *5*(12), 1468–1483.

Allen, C. D., et al. (2010), A global overview of drought and heat-induced tree mortality reveals emerging climate change risks for forests, *For. Ecol. Manage.*, *259*(4), 660–684.

Ashfaq, M., C. B. Skinner, and N. S. Diffenbaugh (2010a), Influence of SST biases on future climate change projections, *Clim. Dyn.*, doi:10.1007/s00382-00010-00875-00382.

Ashfaq, M., L. C. Bowling, K. Cherkauer, J. S. Pal, and N. S. Diffenbaugh (2010b), Influence of climate model biases and daily-scale temperature and precipitation events on hydrological impacts assessment: A case study of the United States, *J. Geophys. Res.*, *115*, D14116, doi:10.1029/2009JD012965.

Barnett, T. P., J. C. Adam, and D. P. Lettenmaier (2005), Potential impacts of a warming climate on water availability in snow-dominated regions, *Nature*, *438*(7066), 303–309.

Barnett, T. P., et al. (2008), Human-induced changes in the hydrology of the western United States, *Science*, *319*(5866), 1080–1083.

Beyene, T., D. P. Lettenmaier, and P. Kabat (2010), Hydrologic impacts of climate change on the Nile River Basin: Implications of the 2007 IPCC scenarios, *Clim. Change*, *100*(3-4), 433–461.

Bohr, G. S., and E. Aguado (2001), Use of April 1 SWE measurements as estimates of peak seasonal snowpack and total cold-season precipitation, *Water Resour. Res.*, *37*(1), 51–60.

Bonfils, C., et al. (2008), Detection and attribution of temperature changes in the mountainous western United States, *J. Clim.*, *21*(23), 6404–6424.

Brakebill, J. W., D. M. Wolock, and S. E. Terziotti (2011), Digital hydrologic networks supporting applications related to spatially referenced regression modeling, *J. Am. Water Resour. As.*, *47*(5), 916–932.

Breshears, D. D., et al. (2005), Regional vegetation die-off in response to global-change-type drought, *Proc. Natl. Acad. Sci. U. S. A.*, *102*(42), 15,144–15,148.

Cane, M. A. (2010), Decadal predictions in demand, *Nat. Geosci.*, *3*(4), 231–232.

Carter, T. R., R. N. Jones, X. Lu, S. Bhadwal, C. Conde, L. O. Mearns, B. C. O'Neill, M. D. A. Rounsevell, and M. B. Zurek (2007), New assessment methods and the characterisation of future conditions, in *Climate Change 2007: Impacts, Adaptation and Vulnerability. Contribution of Working Group II to the Fourth Assessment Report of the Intergovernmental Panel on Climate Change*, edited by M. L. Parry et al., pp. 133–171, Cambridge Univ. Press, Cambridge, U.K.

Casola, J. H., L. Cuo, B. Livneh, D. P. Lettenmaier, M. T. Stoelinga, P. W. Mote, and J. M. Wallace (2009), Assessing the impacts of global warming on snowpack in the Washington Cascades, *J. Clim.*, *22*(10), 2758–2772.

Cayan, D. R., S. A. Kammerdiener, M. D. Dettinger, J. M. Caprio, and D. H. Peterson (2001), Changes in the onset of spring in the western United States, *Bull. Am. Meteorol. Soc.*, *82*(3), 399–415.

Cherkauer, K. A., L. C. Bowling, and D. P. Lettenmaier (2003), Variable infiltration capacity cold land process model updates, *Global Planet. Change*, *38*(1-2), 151–159.

Christensen, N. S., and D. P. Lettenmaier (2007), A multimodel ensemble approach to assessment of climate change impacts on the hydrology and water resources of the Colorado River Basin, *Hydrol. Earth Syst. Sc.*, *11*(4), 1417–1434.

Christensen, N. S., A. W. Wood, N. Voisin, D. P. Lettenmaier, and R. N. Palmer (2004), The effects of climate change on the hydrology and water resources of the Colorado River basin, *Clim. Change*, *62*(1-3), 337–363.

Clark, R. T., J. M. Murphy, and S. J. Brown (2010), Do global warming targets limit heatwave risk?, *Geophys. Res. Lett.*, *37*, L17703, doi:10.1029/2010GL043898.

Costa-Cabral, M., S. B. Roy, E. P. Maurer, W. B. Mills, and L. M. Chen (2013), Snowpack and runoff response to climate change in Owens Valley and Mono Lake watersheds, *Clim. Change*, *116*(1), 97–109.

Daly, C., G. H. Taylor, W. P. Gibson, T. W. Parzybok, G. L. Johnson, and P. A. Pasteris (2000), High-quality spatial climate data sets for the United States and beyond, *Trans. Asae*, *43*(6), 1957–1962.

Das, T., H. G. Hidalgo, M. D. Dettinger, D. R. Cayan, D. W. Pierce, C. Bonfils, T. P. Barnett, G. Bala, and A. Mirin (2009), Structure and detectability of trends in hydrological measures over the western United States, *J. Hydrometeorol.*, *10*(4), 871–892.

Das, T., D. W. Pierce, D. R. Cayan, J. A. Vano, and D. P. Lettenmaier (2011), The importance of warm season warming to western US streamflow changes, *Geophys. Res. Lett.*, *38*, L23403, doi:10.1029/2011GL049660.

de la Fuente, A., N. Bing, I. Hoeschele, and P. Mendes (2004), Discovery of meaningful associations in genomic data using partial correlation coefficients, *Bioinformatics*, *20*(18), 3565–3574.

Deser, C., A. Phillips, V. Bourdette, and H. Y. Teng (2012), Uncertainty in climate change projections: The role of internal variability, *Clim. Dyn.*, *38*(3-4), 527–546.

Dettinger, M. D., and D. R. Cayan (1995), Large-scale atmospheric forcing of recent trends toward early snowmelt runoff in California, *J. Clim.*, *8*(3), 606–623.

Dickinson, R. E., A. Henderson-Sellers, and P. J. Kennedy (1993), *Biosphere-Atmosphere Transfer Scheme (BATS) Version 1e as Coupled to the NCAR Community Climate Model*, National Center for Atmospheric Research, Boulder, CO.

Diffenbaugh, N. S., and M. Ashfaq (2007), Response of California current forcing to mid-Holocene insolation and sea surface temperature, *Paleoceanography*, *22*, PA3101, doi:10.1029/2006PA001382.

Diffenbaugh, N. S., and M. Ashfaq (2010), Intensification of hot extremes in the United States, *Geophys. Res. Lett.*, *37*, L15701, doi:10.1029/2010GL043888.

Diffenbaugh, N. S., and M. Scherer (2011), Observational and model evidence of global emergence of permanent, unprecedented heat in the 20th and 21st centuries, *Clim. Change*, doi:10.1007/s10584-10011-10112-y.

Diffenbaugh, N. S., and M. Scherer (2013), Using climate impacts indicators to evaluate climate model ensembles: Temperature suitability of premium winegrape cultivation in the United States, *Clim. Dyn.*, *40*(3-4), 709–729.

Diffenbaugh, N. S., J. S. Pal, R. J. Trapp, and F. Giorgi (2005), Fine-scale processes regulate the response of extreme events to global climate change, *Proc. Natl. Acad. Sci. U. S. A.*, *102*(44), 15,774–15,778.

Diffenbaugh, N. S., M. Ashfaq, B. Shuman, J. W. Williams, and P. J. Bartlein (2006), Summer aridity in the United States: Response to mid-Holocene changes in insolation and sea surface temperature, *Geophys. Res. Lett.*, *33*, L22712, doi:10.1029/2006GL028012.

Diffenbaugh, N. S., M. Ashfaq, and M. Scherer (2011), Transient regional climate change: Analysis of the summer climate response in a high-resolution, century-scale ensemble experiment over the continental United States, *J. Geophys. Res.*, *116*(D24), D24111, doi:10.1029/2011JD016458.

Diffenbaugh, N. S., M. Scherer, and M. Ashfaq (2013), Response of snow-dependent hydrologic extremes to continued global warming, *Nature Clim. Change*, *3*(4), 379–384.

Fan, Y., H. M. van den Dool, and W. Wu (2011), Verification and intercomparison of multimodel simulated land surface hydrological datasets over the United States, *J. Hydrometeorol.*, *12*(4), 531–555.

Fritsch, J. M., and C. F. Chappell (1980), Numerical prediction of convectively driven mesoscale pressure systems. Part I: Convective parameterization, *J. Atmos. Sci.*, *37*, 1722–1733.

Gao, Y. H., J. A. Vano, C. M. Zhu, and D. P. Lettenmaier (2011), Evaluating climate change over the Colorado River basin using regional climate models, *J. Geophys. Res.*, *116*, D13104, doi:10.1029/2010JD015278.

Grell, G. A. (1993), Prognostic evaluation of assumptions used by cumulus parameterizations, *Mon. Weather Rev.*, *121*, 764–787.

Grell, G. A., J. Dudhia, and D. R. Stauffer (1994), Description of the fifth generation Penn State/NCAR Mesoscale Model (MM5), *Technical Report TN-398 + STR*, 121 pp., National Center for Atmospheric Research, Boulder, CO.

Hamlet, A. F., and D. P. Lettenmaier (1999), Effects of climate change on hydrology and water resources in the Columbia River basin, *J. Am. Water Resour. Assoc.*, *35*(6), 1597–1623.

Hamlet, A. F., P. W. Mote, M. P. Clark, and D. P. Lettenmaier (2005), Effects of temperature and precipitation variability on snowpack trends in the western United States, *J. Clim.*, *18*(21), 4545–4561.

Hawkins, E., and R. Sutton (2010), The potential to narrow uncertainty in projections of regional precipitation change, *Clim. Dyn.*, doi:10.1007/s00382-00010-00810-00386.

Hayhoe, K., et al. (2004), Emissions pathways, climate change, and impacts on California, *Proc. Natl. Acad. Sci. U. S. A.*, *101*(34), 12,422–12,427.

Holtslag, A. A. M., E. I. F. de Bruijn, and H. L. Pan (1990), A high resolution air mass transformation model for short-range weather forecasting, *Mon. Weather Rev.*, *118*, 1561–1575.

Jordan, R. (1991), A One-Dimensional Temperature Model for a Snow Cover: Technical Documentation for SNTHERM.89*Rep.*, 61 pp, Cold Regions Research and Engineering Laboratory.

Kapnick, S., and A. Hall (2012), Causes of recent changes in western North American snowpack, *Clim. Dyn.*, *38*(9-10), 1885–1899.

Kelly, A. E., and M. L. Goulden (2008), Rapid shifts in plant distribution with recent climate change, *Proc. Natl. Acad. Sci. U. S. A.*, *105*(33), 11,823–11,826.

Kiehl, J. T., J. J. Hack, G. B. Bonan, B. A. Boville, B. P. Briegleb, D. L. Williamson, and P. J. Rasch (1996), Description of the NCAR Community Climate Model (CCM3), *Technical Report TN-420 + STR*, 152 pp., National Center for Atmospheric Research, Boulder, CO.

Kurz, W. A., C. C. Dymond, G. Stinson, G. J. Rampley, E. T. Neilson, A. L. Carroll, T. Ebata, and L. Safranyik (2008), Mountain pine beetle and forest carbon feedback to climate change, *Nature*, *452*(7190), 987–990.

Leung, L. R., and S. J. Ghan (1999), Pacific northwest climate sensitivity simulated by a regional climate model driven by a GCM. Part II: 2xCO (2) simulations, *J. Clim.*, *12*(7), 2031–2053.

Leung, L. R., Y. Qian, X. D. Bian, W. M. Washington, J. G. Han, and J. O. Roads (2004), Mid-century ensemble regional climate change scenarios for the western United States, *Clim. Change*, *62*(1-3), 75–113.

Liang, X., D. P. Lettenmaier, E. F. Wood, and S. J. Burges (1994), A simple hydrologically based model of land surface water and energy fluxes for general circulation models, *J. Geophys. Res.*, *99*(D7), 14,415–14,428.

Matthews, H. D., and K. Caldeira (2008), Stabilizing climate requires near-zero emissions, *Geophys. Res. Lett.*, *35*, L04705, doi:10.1029/2007GL032388.

Matthews, H. D., and A. J. Weaver (2010), Committed climate warming, *Nat. Geosci.*, *3*(3), 142–143.

Maurer, E. P. (2007), Uncertainty in hydrologic impacts of climate change in the Sierra Nevada, California, under two emissions scenarios, *Clim. Change*, *82*(3-4), 309–325.

McCabe, G. J., and M. P. Clark (2005), Trends and variability in snowmelt runoff in the western United States, *J. Hydrometeorol.*, *6*(4), 476–482.

Mearns, L. O., W. J. Gutowski, R. Jones, L.-Y. Leung, S. McGinnis, A. M. B. Nunes, and Y. Qian (2009), A regional climate change assessment program for North America, *Eos Trans. AGU*, *90*(36), 311–312.

Meehl, G. A., W. M. Washington, B. D. Santer, W. D. Collins, J. M. Arblaster, A. Hu, D. M. Lawrence, H. Teng, L. E. Buja, and W. G. Strand (2006), Climate change projections for the twenty-first century and climate change commitment in the CCSM3, *J. Clim.*, *19*, 2597–2616.

Meehl, G. A., C. Covey, T. Delworth, M. Latif, B. McAvaney, J. F. B. Mitchell, R. J. Stouffer, and K. E. Taylor (2007a), The WCRP CMIP3 multimodel dataset—A new era in climate change research, *Bull. Am. Meteorol. Soc.*, *88*(9), 1383–1394.

Meehl, G. A., et al. (2007b), Global climate projections, in *Climate Change 2007: The Physical Science Basis. Contribution of Working Group I to the Fourth Assessment Report of the Intergovernmental Panel on Climate Change*, edited by S. Solomon et al., pp. 747–845, Cambridge University Press, Cambridge, United Kingdom and New York, NY, USA.

Mock, C. J. (1996), Climatic controls and spatial variations of precipitation in the western United States, *J. Clim.*, *9*(5), 1111–1125.

Moore, J. N., J. T. Harper, and M. C. Greenwood (2007), Significance of trends toward earlier snowmelt runoff, Columbia and Missouri Basin headwaters, western United States, *Geophys. Res. Lett.*, *34*, L16402, doi:10.1029/2007GL031022.

Mote, P. W. (2006), Climate-driven variability and trends in mountain snowpack in western North America, *J. Clim.*, *19*, 6209–6220.

Mote, P. W., A. F. Hamlet, M. P. Clark, and D. P. Lettenmaier (2005), Declining mountain snowpack in western North America, *Bull. Am. Meteorol. Soc.*, *86*(1), 39.

Murphy, J. M., D. M. H. Sexton, D. N. Barnett, G. S. Jones, M. J. Webb, M. Collins, and D. A. Stainforth (2004), Quantification of modelling uncertainties in a large ensemble of climate change simulations, *Nature*, *430*(7001), 768–772.

Myers, N., R. A. Mittermeier, C. G. Mittermeier, G. A. B. da Fonseca, and J. Kent (2000), Biodiversity hotspots for conservation priorities, *Nature*, *403*(6772), 853–858.

Pal, J. S., E. E. Small, and E. A. B. Eltahir (2000), Simulation of regional-scale water and energy budgets: Representation of subgrid cloud and precipitation processes within RegCM, *J. Geophys. Res.*, *105*(D24), 29,579–29,594.

Pal, J. S., et al. (2007), Regional climate modeling for the developing world: The ICTP RegCM3 and RegCNET, *Bull. Am. Meteorol. Soc.*, *89*(9), 1395–1409.

Park Williams, A., et al. (2013), Temperature as a potent driver of regional forest drought stress and tree mortality, *Nature Clim. Change*, *3*(3), 292–297.

Payne, J. T., A. W. Wood, A. F. Hamlet, R. N. Palmer, and D. P. Lettenmaier (2004), Mitigating the effects of climate change on the water resources of the Columbia River Basin, *Clim. Change*, *62*(1-3), 233–256.

Peters, G. P., R. M. Andrew, T. Boden, J. G. Canadell, P. Ciais, C. Le Quere, G. Marland, M. R. Raupach, and C. Wilson (2013), The challenge to keep global warming below 2 °C, *Nature Clim. Change*, *3*(1), 4–6.

Pierce, D. W., and D. R. Cayan (2013), The uneven response of different snow measures to human-induced climate warming, *J. Clim.*, *26*(12), 4,148–4,167.

Pierce, D. W., et al. (2008), Attribution of declining western US snowpack to human effects, *J. Clim.*, *21*(23), 6425–6444.

Rasmussen, R., et al. (2011), High-resolution coupled climate runoff simulations of seasonal snowfall over Colorado: A process study of current and warmer climate, *J. Clim.*, *24*(12), 3015–3048.

Rauscher, S. A., J. S. Pal, N. S. Diffenbaugh, and M. M. Benedetti (2008), Future changes in snowmelt-driven runoff timing over the western US, *Geophys. Res. Lett.*, *35*, L16703, doi:10.1029/2008GL034424.

Rood, S. B., G. M. Samuelson, J. K. Weber, and K. A. Wywrot (2005), Twentieth-century decline in streamflows from the hydrographic apex of North America, *J. Hydrol.*, *306*(1-4), 215–233.

Rood, S. B., J. Pan, K. M. Gill, C. G. Franks, G. M. Samuelson, and A. Shepherd (2008), Declining summer flows of Rocky Mountain rivers: Changing seasonal hydrology and probable impacts on floodplain forests, *J. Hydrol.*, *349*(3-4), 397–410.

Scherrer, S. C., C. Appenzeller, and M. Laternser (2004), Trends in Swiss Alpine snow days: The role of local- and large-scale climate variability, *Geophys. Res. Lett.*, *31*, L13215, doi:10.1029/2004GL020255.

Scully, R. A. (2010), *Intercomparison of PRISM and Daymet Temperature Interpolation from 1980 to 2003*, Utah State University, All Graduate Theses and Dissertations. Paper 578, http://digitalcommons.usu.edu/etd/578.

Seaber, P. R., F. P. Kapinos, and G. L. Knapp (1987), Hydrologic unit maps, Water Supply Paper No. 2294 *Rep.*, 61 pp. pp, U.S. Geological Survey, Denver, CO.

Solomon, S., G.-K. Plattner, R. Knutti, and P. Friedlingstein (2009), Irreversible climate change due to carbon dioxide emissions, *Proceedings of the National Academy of Sciences*.

Stewart, I. T. (2009), Changes in snowpack and snowmelt runoff for key mountain regions, *Hydrol. Processes*, *23*(1), 78–94.

Stewart, I. T., D. R. Cayan, and M. D. Dettinger (2004), Changes in snowmelt runoff timing in western North America under a 'business as usual' climate change scenario, *Clim. Change*, *62*(1-3), 217–232.

Sun, S., J. Jin, and Y. Xue (1999), A simple snow-atmosphere-soil transfer model, *J. Geophys. Res.*, *104*(D16), 19,587–19,597.

Trapp, R. J., N. S. Diffenbaugh, H. E. Brooks, M. E. Baldwin, E. D. Robinson, and J. S. Pal (2007), Changes in severe thunderstorm environment frequency during the 21st century caused by anthropogenically enhanced global radiative forcing, *Proc. Natl. Acad. Sci. U. S. A.*, *104*(50), 19,719–19,723.

Trapp, R. J., N. S. Diffenbaugh, and A. Gluhovsky (2009), Transient response of severe thunderstorm forcing to elevated greenhouse gas concentrations, *Geophys. Res. Lett.*, *36*, L01703, doi:10.1029/2008GL036203.

USCB (2011), U.S. Census Bureau, State and County QuickFacts, http://quickfacts.census.gov/qfd/states/06000.html.

USDA, E. R. S. (2011), Farm Income: Data Files, http://www.ers.usda.gov/data/FarmIncome/FinfidmuXls.htm (2009 data)*Rep*.

Vano, J. A., T. Das, and D. P. Lettenmaier (2012), Hydrologic sensitivities of Colorado River runoff to changes in precipitation and temperature, *J. Hydrometeorol.*, *13*(3), 932–949.

Vicuna, S., E. P. Maurer, B. Joyce, J. A. Dracup, and D. Purkey (2007), The sensitivity of California water resources to climate change scenarios, *J. Am. Water Resour. Assoc.*, *43*(2), 482–498.

WAC (2010), WAC 246-290-100, Water system plan, Washington State Legislature, http://apps.leg.wa.gov/wac/default.aspx?cite=246-290-100, edited.

Walker, M. D., and N. S. Diffenbaugh (2009), Evaluation of high-resolution simulations of daily-scale temperature and precipitation over the United States, *Clim. Dyn.*, doi:10.1007/s00382-00009-00603-y.

Westerling, A. L., H. G. Hidalgo, D. R. Cayan, and T. W. Swetnam (2006), Warming and earlier spring increase western US forest wildfire activity, *Science*, *313*(5789), 940–943.

Wi, S., F. Dominguez, M. Durcik, J. Valdes, H. F. Diaz, and C. L. Castro (2012), Climate change projection of snowfall in the Colorado River Basin using dynamical downscaling, *Water Resour. Res.*, *48*, W05504, doi:10.1029/2011WR010674.

Wigley, T. M. L. (2005), The climate change commitment, *Science*, *307*(5716), 1766–1769.